


ORIGINAL PAPER

Open Access

# Earthquakes in Switzerland and surrounding regions during 2017 and 2018



Tobias Diehl<sup>1\*</sup> , John Clinton<sup>1</sup>, Carlo Cauzzi<sup>1</sup>, Toni Kraft<sup>1</sup>, Philipp Kästli<sup>1</sup>, Nicolas Deichmann<sup>1</sup>, Frédéric Massin<sup>1</sup>, Francesco Grigoli<sup>1</sup>, Irene Molinari<sup>2,3</sup>, Maren Böse<sup>1</sup>, Manuel Hobiger<sup>1</sup>, Florian Haslinger<sup>1</sup>, Donat Fäh<sup>1</sup> and Stefan Wiemer<sup>1</sup>

## Abstract

This report summarizes the seismicity in Switzerland and surrounding regions in the years 2017 and 2018. In 2017 and 2018, the Swiss Seismological Service detected and located 1227 and 955 earthquakes in the region under consideration, respectively. The strongest event in the analysed period was the  $M_L$  4.6 Urnerboden earthquake, which occurred in the border region of cantons Uri, Glarus and Schwyz on March 6, 2017. The event was the strongest earthquake within Switzerland since the  $M_L$  5.0 Vaz earthquake of 1991. Associated ground motions indicating intensity IV were reported in a radius up to about 50 km and locally approached intensity VI in the region close to the epicentre. Derived focal mechanisms and relative hypocentre relocations of the immediate aftershocks image a NNW–SSE striking sinistral strike-slip fault. Together with other past events in this region, the Urnerboden earthquake suggests the existence of a system of sub-parallel strike-slip faults, likely within in the uppermost crystalline basement of the eastern Aar Massif. A vigorous earthquake sequence occurred close to Château-d'Oex in the Préalpes-Romandes region in western Switzerland. With a magnitude of  $M_L$  4.3, the strongest earthquake of the sequence occurred on July 1, 2017. Focal mechanism and relative relocations of fore- and aftershocks image a NNE dipping normal fault in about 4 km depth. Two similarly oriented shallow normal-fault events occurred between subalpine Molasse and Préalpes units close to Châtel-St-Denis and St. Silvester in 2017/18. Together, these events indicate a domain of NE–SW oriented extensional to transtensional deformation along the Alpine Front between Lake Geneva in the west and the Fribourg Fault in the east. The structural complexity of the Fribourg Fault is revealed by an  $M_L$  2.9 earthquake near Tifers in 2018. The event images a NW–SE striking fault segment within the crystalline basement, which might be related to the Fribourg Fault Zone. Finally, the  $M_L$  2.8 Grenchen earthquake of 2017 provides a rare example of shallow thrust faulting along the Jura fold-and-thrust belt, indicating contraction in the northwestern Alpine foreland of Switzerland.

## Zusammenfassung

Dieser Bericht stellt eine Zusammenfassung der im Jahr 2017 und 2018 in der Schweiz und Umgebung aufgetretenen Erdbeben dar. Im Jahr 2017 erfasste und lokalisierte der Schweizerische Erdbebendienst im erwähnten Untersuchungsgebiet 1227 Erdbeben. Im Jahr 2018 lag diese Zahl bei 955 Erdbeben. Das stärkste Ereignis im untersuchten Zeitraum war das  $M_L$  4.6 Urnerboden Beben, welches sich am 6. März 2017 im Grenzgebiet der Kantone Uri, Glarus

Editorial handling: Stefan Schmid.

\*Correspondence: tobias.diehl@sed.ethz.ch

<sup>1</sup> Swiss Seismological Service, ETH Zürich, Sonneggstrasse 5, 8092 Zürich, Switzerland

Full list of author information is available at the end of the article



© The Author(s) 2021. This article is licensed under a Creative Commons Attribution 4.0 International License, which permits use, sharing, adaptation, distribution and reproduction in any medium or format, as long as you give appropriate credit to the original author(s) and the source, provide a link to the Creative Commons licence, and indicate if changes were made. The images or other third party material in this article are included in the article's Creative Commons licence, unless indicated otherwise in a credit line to the material. If material is not included in the article's Creative Commons licence and your intended use is not permitted by statutory regulation or exceeds the permitted use, you will need to obtain permission directly from the copyright holder. To view a copy of this licence, visit <http://creativecommons.org/licenses/by/4.0/>.

und Schwyz ereignete. Das Urnerboden Beben war das stärkste Ereignis innerhalb der Schweiz seit dem  $M_L$  5.0 Beben bei Vaz im Jahre 1991. Nahe dem Epizentrum erreichten die verursachten Bodenbewegungen eine makroseismische Intensität der Stufe VI, und in einem Umkreis von bis zu 50 km wurden Intensitäten der Stufe IV verspürt. Herdmechanismen und Relativlokalisierungen von unmittelbaren Nachbeben deuten auf eine NNW–SSO streichende, sinistrale Blattverschiebung hin. Ähnlichkeiten mit weiteren Beben in der jüngeren Vergangenheit in dieser Region weisen auf ein System von subparallelen Blattverschiebungen im obersten Teil des kristallinen Grundgebirges des östlichen Aar Massivs hin. Eine außergewöhnlich starke Sequenz von Erdbeben ereignete sich zudem nahe Château-d'Oex, in der Region Préalpes-Romandes im Westen der Schweiz. Mit einer Magnitude von  $M_L$  4.3 ereignete sich das stärkste Beben dieser Serie am 1. Juli 2017. Herdmechanismen und Relativlokalisierungen von Vor- und Nachbeben deuten auf eine nach NNO einfallende Abschiebung in ungefähr 4 km Tiefe hin. Zwei weitere, ähnlich orientierte Abschiebungsbeben traten im Zeitraum 2017/18 nahe Châtel-St-Denis und St. Silvester im Bereich zwischen Subalpiner Molasse und den Préalpes Decken auf. Zusammengefasst deuten diese drei Abschiebungsbeben auf einen Bereich von NO-SW gerichteter Extension bzw. Transtension entlang der Alpenfront hin, welcher durch den Genfersee im Westen und der Fribourg-Verwerfung im Osten begrenzt ist. Ein  $M_L$  2.9 Beben bei Tavers im Jahr 2018 erlaubt neue Einblicke in die komplexe Struktur der Fribourg Störung. Das Beben weist auf ein NW-SO streichendes Verwerfungssegment im kristallinen Grundgebirge hin, das eventuell im Zusammenhang mit der Fribourg Verwerfung steht. Das  $M_L$  2.8 Erdbeben, das sich im Jahr 2017 nahe Grenchen ereignete, stellt zudem ein seltenes Beispiel einer seismisch aktiven Überschiebung südlich des Faltenjuras im nordwestlichen alpinen Vorland der Schweiz dar.

## Résumé

Ce rapport résume l'activité sismique en Suisse et dans les régions limitrophes au cours des années 2017 et 2018. En 2017 et 2018, le Service Sismologique Suisse a détecté et localisé respectivement 1227 et 955 séismes dans la zone considérée. L'événement le plus puissant dans la période analysée fut le séisme d'Urnerboden de magnitude  $M_L$  4.6, qui s'est produit le 6 mars 2017 dans la région frontalière des cantons d'Uri, de Glaris et Schwytz. Ce fut le plus grand séisme en Suisse depuis le séisme de magnitude  $M_L$  5.0 à Vaz en 1991. Les mouvements du sol associés au séisme d'Urnerboden approchèrent une intensité maximale de VI, et une intensité de IV fut reportée à une distance d'environ 50 km. Les mécanismes au foyer et les relocalisations relatives des hypocentres de répliques rendent compte d'une faille décrochante senestre de direction NNW–SSE. Le séisme d'Urnerboden et la sismicité historique environnante suggèrent l'existence de failles décrochantes sub-parallèles, probablement dans la partie supérieure du socle cristallin à l'extrémité orientale du massif de l'Aar. Une autre séquence remarquable s'est produite près de Château-d'Oex dans les Préalpes romandes en Suisse occidentale. Le plus puissant séisme de cette séquence s'est produit le 1er juillet 2017 avec une magnitude  $M_L$  de 4.3. Les mécanismes au foyer et les relocalisations relatives de ses précurseurs et répliques permettent de visualiser une faille normale avec un pendage vers le NNE à environ 4 km de profondeur. Deux événements associés à des failles normales superficielles d'orientation similaires se sont produits en 2017 et 2018, entre les Molasses sub-alpines et les unités structurales des Préalpes, près de Châtel-St-Denis et St. Silvestre. L'ensemble de ces événements indiquent le long du front alpin, entre le lac Léman à l'ouest et la faille de Fribourg à l'est, un domaine NE–SW où s'opère une transition de déformation entre une région d'extension et une région de transtension. La complexité structurale de cette dernière est révélée par un séisme d'une magnitude  $M_L$  2.9 près de Tavel en 2018. Cet événement décrit un segment de faille NW–SE au sein du socle cristallin, qui pourrait être relié à la zone de faille de Fribourg. Enfin, le séisme de magnitude  $M_L$  2.8 à Grenchen en 2017 procure une information rare sur la dynamique active de la partie superficielle de la ceinture de chevauchement du Jura dans l'avant-pays nord-ouest-alpin Suisse.

**Keywords:** Seismicity, Focal mechanisms, Seismotectonics, Urnerboden, Aar Massif, Château-d'oex, Préalpes, Fribourg, Jura fold-and-thrust belt

## 1 Introduction

Past earthquake activity in Switzerland and surrounding regions has been documented in a series of annual reports since 1879. A detailed overview on the history of past reports and studies covering different aspects of the

recent seismicity of Switzerland is provided e.g. by Diehl et al. (2014). The present report first summarizes the state of the seismic network and documents changes in its configuration during 2017 and 2018. Then we provide a short overview of the methods used for earthquake analysis.

This is followed by a description of the seismic activity and significant earthquakes in 2017/18. The discussion of significant earthquakes and earthquake sequences considers information from derived focal mechanisms and high-precision relative hypocentre relocations.

## 2 Data acquisition, analysis and access

### 2.1 Seismic stations in operation during 2017/18

The Swiss Seismological Service at ETH Zurich (SED) operates two nationwide seismic networks, a high-gain (weak-motion) network predominantly consisting of broad-band seismometers (SDSNet, Additional file 1: Table S1) that is often complimented by co-located accelerometers, and a low-gain (strong-motion) network (SSMNet, Additional file 1: Table S2) that consists of accelerometers (Swiss Seismological Service (SED) at ETH Zurich 1983). A more complete description can be found in previous Annual Reports (e.g., Diehl et al. 2014). In addition, the SED operates a number of temporary stations for various projects (Additional file 1: Table S3). SED-operated permanent stations with on-line data acquisition that were operational at the end of 2018 are shown in Fig. 1.

Within the Swiss Strong Motion Network (SSMNet) renewal project, 100 free-field, real-time, very broad-band accelerometer stations are being installed over a 10-year timeframe between 2010 and 2021 (e.g., Clinton et al. 2011). In 2017/18, 15 new accelerometer stations were installed (Fig. 1; 8 in 2017: SCHAT, SEFS, SGLK, SHER, SRFW, SNTZ, SUSI, SZWD2; 7 in 2018: SAARA, SARC, SBUL, SENGL, SFRS, SMELS, SWYZ).

The broadband weak-motion seismometer network is also undergoing a renewal period that continued during 2017 and 2018. Numerous stations were upgraded by replacement of the acquisition hardware and broadband seismometers, and if not already existing, the addition of an accelerometer. In 2018, a new broadband weak-motion station JAUN was installed close to Jaun (FR). To improve seismic monitoring in regions of past or future geothermal projects, five new broadband weak-motion stations were installed in 2017/18 (Fig. 1; FULLY, ILLEZ, LAVEY, SAVIG, SGT18). In 2017, stations at LKBD (Leukerbad) and GSF01 (Oberhasli) were dismantled. Further, all first-generation dial-up analogue accelerometer stations were decommissioned in 2017.

As part of various projects, several new semi-permanent stations have been installed to locally improve the density of the network in 2017/18 (e.g. in the region of the Bedretto Underground Laboratory for Geoenergies and the Geneva basin). The networks built to monitor potential sites for radioactive waste disposal; the geothermal projects in Basel (2006) and Sankt Gallen (2013); and the Mont Terri Rock Laboratories continue to operate.

Surface stations related to the Grimsel Rock Laboratory were partly dismantled. In 2017/18, the temporary stations from the AlpArray Seismic Network (AASN) (Molinari et al. 2016; AlpArray Seismic Network 2015) continue to operate in the greater Alpine region, including three stations in Switzerland (A060A/B, A061A, and A062A). The number of AlpArray stations operating outside but near the Swiss border in Italy, France, Austria and Germany is significant, and these stations are included in the national monitoring when possible. To improve the reliability of locations for events at the periphery of or outside of Switzerland, the SED continues to be engaged in an on-going cross-frontier cooperative effort to exchange seismic data in real-time with foreign seismic networks as documented in detail by Diehl et al. (2014). Over 60 foreign stations were monitored by the SED at the end of 2018.

The SED now provides open access to station inventory, waveform data and earthquakes catalogues via the International Federation of Digital Seismograph Networks (FDSN) webservices, the community standard (see <http://www.seismo.ethz.ch/en/research-and-teaching/products-software/fdsn-web-services/> for details).

### 2.2 Automatic earthquake detection and magnitude of completeness during 2017/18

All stations with real-time data acquisition (Fig. 1) were used for automatic real-time detection of seismic events. An estimation of the magnitude of completeness ( $M_C$ ) achieved by the network configuration at the end of 2018 is shown in Fig. 1. The  $M_C$  magnitude is defined as the lowest magnitude of events that a network is able to record reliably and completely (e.g., Schorlemmer and Woessner 2008). We use the probabilistic approach of Schorlemmer and Woessner (2008) to compute lateral variations in  $M_C$  (see Diehl et al. 2018 for details). The map shown in Fig. 1 assumes a probability of detection of 0.99, a hypothetical focal depth of 5 km and a minimum number of 6 automatic triggers, which corresponds to the minimum number currently required by the monitoring system of the SED (Diehl et al. 2013). Compared to previous  $M_C$  maps of Switzerland (e.g., Nanjo et al. 2010), the recent and ongoing densification of the seismic network has significantly improved the detection capabilities throughout Switzerland. Due to the removal of temporary stations in the Grimsel area,  $M_C$  slightly deteriorated in this region compared to previous estimates (Diehl et al. 2018). On the other hand,  $M_C$  in western and southwestern Switzerland improved compared to previous estimates due to the densification of stations in these regions during 2017/18. The completeness magnitude achieved by the network configuration at the end of 2018 is  $M_C=1.5$  or better for most parts of Switzerland



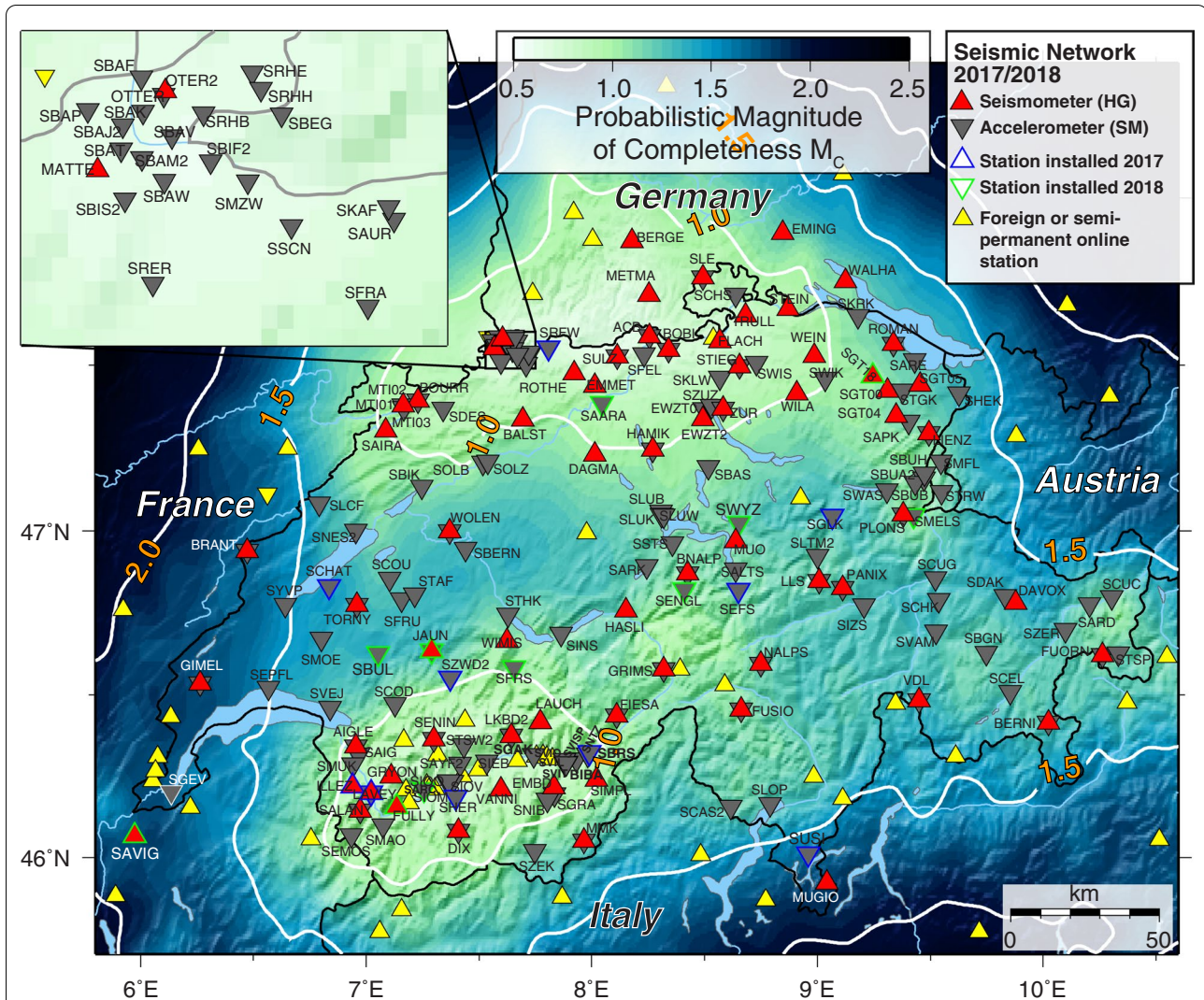


**Fig. 1** Seismograph stations in Switzerland and surrounding regions with on-line data acquisition operational at the end of 2018. Stations of the “Switzerland Seismological Network” (network code “CH”) are indicated with labels. The stations defined as high-gain (HG) are mostly equipped with broad-band or short period (mostly 5 s) seismometers and may also include accelerometers. The strong-motion stations (SM) only have accelerometers (see also Additional file 1: Tables S1–S3). Symbols outlined in blue colour indicate seismometer or accelerometers installed in 2017. Green outline indicates stations installed in 2018. Yellow triangles mark additional permanent or temporary stations with real-time data acquisition that are used to improve detection and location of seismicity. Colours projected onto the topographic relief in the background show the lateral variation of the magnitude of completeness ( $M_C$ ) for on-line stations operating at the end of 2018, assuming a detection probability of 0.99, a minimum number of 6 automatic triggers, and a hypothetical focal depth of 5 km. Bold, white lines indicate  $M_C$  contours of 1.0, 1.5 and 2.0

and around  $M_C = 1.0$  in north and southwest Switzerland (Fig. 1). Regions of relatively higher  $M_C$  are the western Molasse basin and the southwestern Jura Mountains with  $M_C$  between 1.5 and 2.0.

### 2.3 Routine and supplementary earthquake analysis

Methods and software currently used for routine earthquake analysis are described in detail in Diehl et al. (2013, 2014, 2018). Later in this report, we will discuss the ground shaking associated with two major

earthquakes in 2017. Maps of ground shaking are automatically computed by the SED for every earthquake with  $M_L \geq 2.5$  within the greater Swiss region using the USGS ShakeMap software (Worden et al. 2010, 2020). SED ShakeMaps are computed as described in Cauzzi et al. (2015), using the Swiss ground-motion model of Edwards and Fäh (2013), combined with regional site amplification factors (Fäh et al. 2011) and station recordings. Macroseismic intensity according to the European Macroseismic Scale (EMS-98; Grünthal 1998) is converted from measured peak ground velocity using the



equations of Faenza and Michelini (2010). The ShakeMaps presented in the following sections were computed using the new USGS ShakeMap 4.0 software (Worden et al. 2020), which features the improved interpolation method described by Worden et al. (2018) and the ground motion models as implemented in OpenQuake (Pagani et al. 2014).

To enhance the completeness for selected sequences in 2017/18, a cross-correlation based template matching method was implemented in order to lower the detection threshold of micro-seismicity. The applied procedure is described in Herrmann et al. (2019). To resolve active fault planes and to image the spatio-temporal evolution for selected earthquake sequences, we performed relative hypocentre relocations using the double-difference method of Waldhauser and Ellsworth (2000) in combination with waveform cross-correlation. The applied procedure is described in Diehl et al. (2017).

### 3 Seismic activity during 2017 and 2018

#### 3.1 Overview

During 2017, the SED detected and located a total of 1227 earthquakes in the region ranging from 5.8 to 10.8° E and 45.7 to 47.9° N shown in Fig. 2a. Based on criteria such as the time of occurrence, the location, and signal character or on direct communication, 237 additional seismic events were identified as quarry blasts. Magnitude values of the earthquakes recorded in 2017 range from  $M_L$  -0.4 to 4.6 (Fig. 3). During 2018, 955 earthquakes and 229 quarry blasts were detected and located by the SED in the same region (Figs. 2b, 3). The magnitudes of earthquakes in 2018 range from  $M_L$  -0.2 to 4.1 (Fig. 3). The events with  $M_L \geq 2.5$  in 2017/18 are listed in Table 1. The chosen magnitude threshold of  $M_L$  2.5 ensures that the data set is comparable to seismicity in the same magnitude range for previous years (completeness magnitude  $M_C = 2.5$  for Switzerland over the period 1975–2018; Nanjo et al. 2010), and makes sure that the number of unidentified quarry blasts and of mislocated earthquakes is negligible. With a total of 23 and 25 earthquakes of magnitude  $M_L \geq 2.5$ , the seismic activity of potentially felt events in either year was close to the yearly average

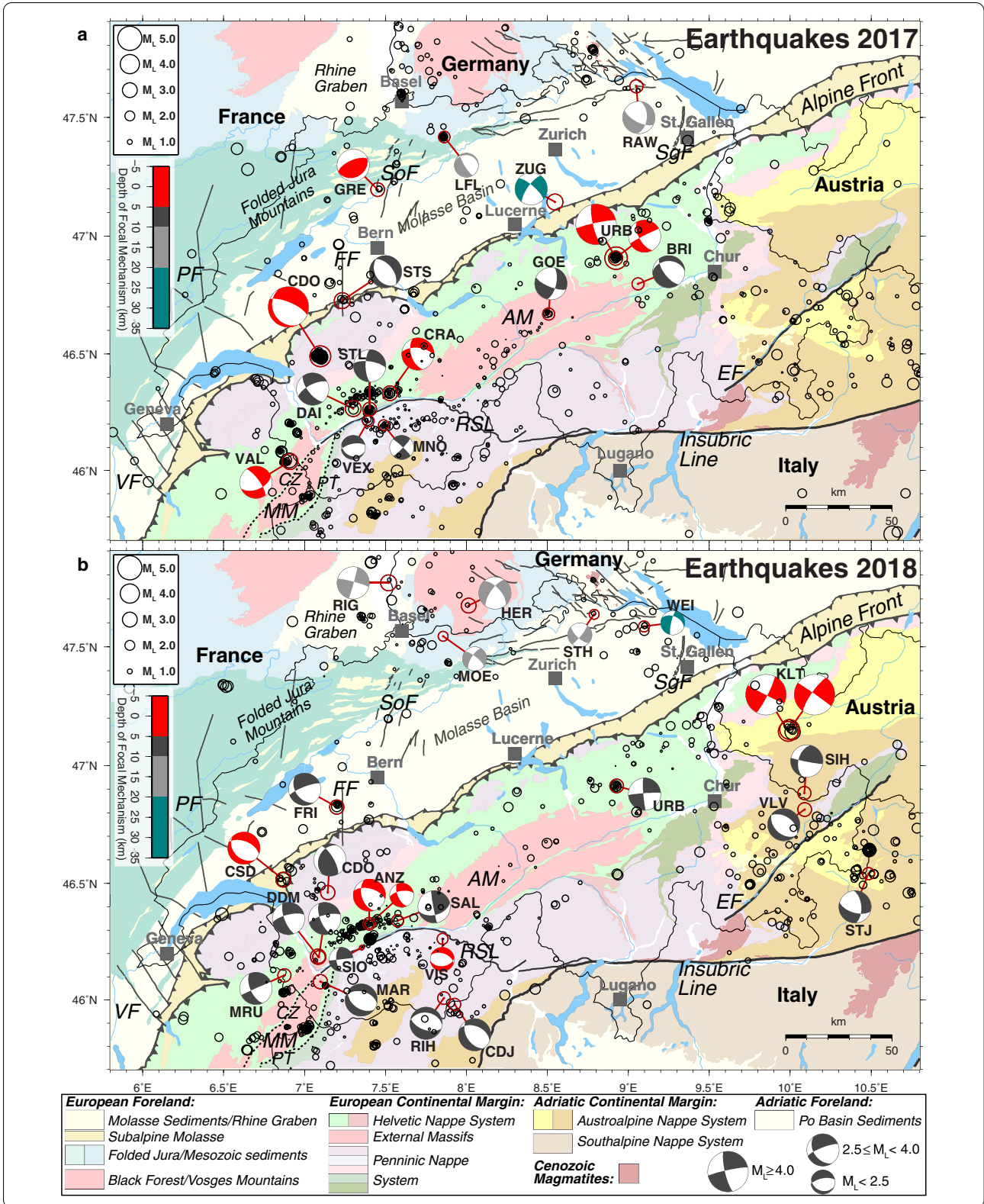
of 23 earthquakes in the same magnitude range over the previous 42 years.

Table 1 includes the location qualities for events with  $M_L \geq 2.5$ . Table 2 documents the criteria used to assign these quality ratings to the given locations, and it also indicates corresponding estimated location uncertainties for each quality value. The location quality criteria as defined in Table 2 provide conservative first-order information on the reliability of epicentre location and focal depth and, since they have been systematically applied in all annual reports since 1999, that allow direct comparison of quality with locations documented in previous annual reports. For events that have occurred since 2013, additional nonlinear location uncertainty estimates can be found in the online catalogue, in XML using the quakeMLformat (<https://quake.ethz.ch/quakeml>). Not all reported uncertainties, however, do account for systematic errors, e.g. errors in the seismic velocity model used for location, or, misidentified phases (e.g., Husen and Hardebeck 2010). Ignoring the contribution of such errors can result in a significant underestimation of the true location accuracy. On the other hand, these errors are difficult to assess (e.g., Husen and Hardebeck 2010). Therefore, we provide realistic uncertainty estimates on hypocentre accuracy in the discussion of significant earthquakes. These estimates consider the nonlinear uncertainty estimates as well as tests with varying subsets of data (P and/or S phases, different distance ranges, with/without refracted Pn phases, etc.) and velocity models.

Fault-plane solutions based on first-motion polarities of all events with  $M_L \geq 2.5$  in 2017/18 are shown in Figs. 2, 4, 5, 6 and 7. The mechanisms derived for selected earthquakes with  $M_L < 2.5$  are shown in Fig. 2 and Additional file 1: Figure S1. All corresponding parameters are summarized in Additional file 1: Table S4. Only well-constrained solutions are listed and first-order uncertainties of the first-motion mechanisms are provided by the spread of solutions in Figs. 4, 5, 6, 7 and Additional file 1: Figure S1. Following the definition of Aki and Richards (2002), the parameters strike, dip and rake are used to define fault-orientations and inferred slip directions in

(See figure on next page.)

**Fig. 2** All epicentres and selected focal mechanisms of earthquakes recorded by the Swiss Seismological Service: **a** during 2017; **b** during 2018. Events and focal mechanisms (lower hemisphere projections) discussed in the text are Göschenen (GOE), Urnerboden (URB), Vallorcine (VAL), Grenchen (GRE), Daillon (DAI), St. Silvester (STS), Château-d'Oex (CDO), Zug (ZUG), Anzère (ANZ), Klostertal (KLT), Herrisried (HER), Rhinegraben (RIG), Châtel-St-Denis (CSD), Dent de Morcles (DDM), Martigny (MAR), Fribourg/Tafers (FRI), and Sion (SIO). Additional events with focal mechanisms are listed in Additional file 1: Table S4. Colour of focal mechanism indicates focal depth. Background colours outline major tectonic units after Swisstopo (2005). Grey solid and dashed lines indicate faults and fault systems. AM Aar Massif, CZ Chamonix/Mont Blanc shear zone, EF Engadine fault, FF Fribourg fault zone, PF Pontarlier fault zone, PT Penninic thrust, RSL Rhone-Simplon Line, SgF St. Gallen fault zone, SoF Solothurn fault zone, VF Vuache fault (Adopted from Egli and Mancktelow (2013), Heuberger et al. (2016), Mock and Herwegh (2017), Vouillamoz, et al. (2017), and Swisstopo (2005))



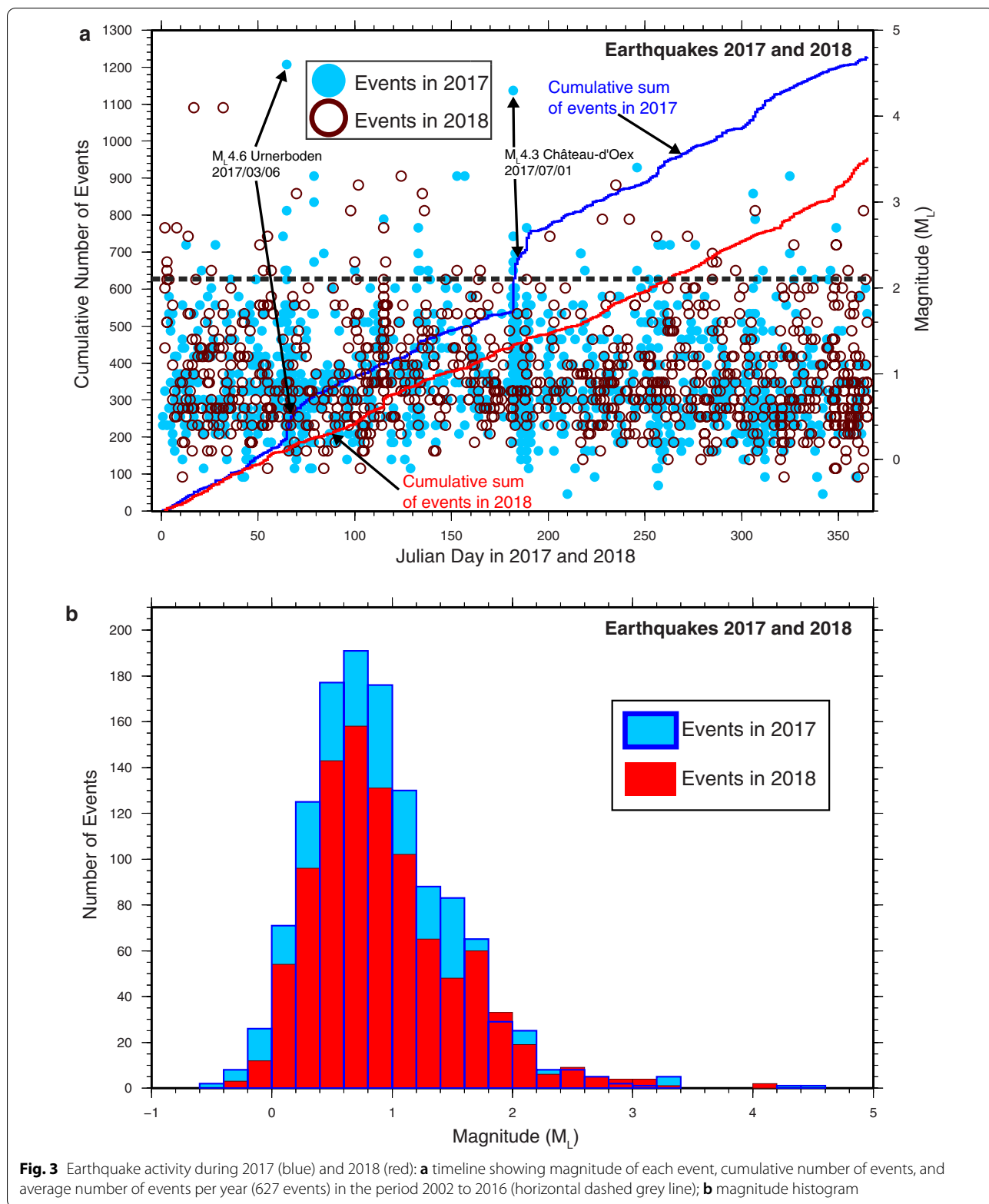


**Fig. 3** Earthquake activity during 2017 (blue) and 2018 (red): **a** timeline showing magnitude of each event, cumulative number of events, and average number of events per year (627 events) in the period 2002 to 2016 (horizontal dashed grey line); **b** magnitude histogram



**Table 1 Earthquakes with  $M_L \geq 2.5$  during 2017 and 2018**

Date and time UTC	Lat. (°N)	Lon. (°E)	X/Y (km)	Z (km)	Mag ( $M_L$ )	Mag ( $M_{WSPEC}$ )	Q	Location
2017/01/13 06:13:14	46.670	8.507	682/169	5	2.5	2.5	B	Göschenen, UR ( <i>GOE</i> )
2017/01/28 13:30:21	46.432	10.019	798/146	8	2.5	2.4	A	Bernina Pass, GR
2017/03/04 01:29:25	47.809	9.415	748/297	21	2.6	2.4	A	Deggenhausertal, D
2017/03/06 20:12:07	46.907	8.925	713/196	4	4.6	4.1	A	Urnerboden, UR ( <i>URB</i> )
2017/03/06 21:57:33	46.908	8.921	713/196	5	2.9	2.7	A	Urnerboden, UR ( <i>URB</i> )
2017/03/20 00:30:55	46.040	6.909	559/099	4	3.3	3.0	A	Vallorcine, F ( <i>VAL</i> )
2017/03/20 21:09:11	46.044	6.905	559/099	4	3.0	2.8	A	Vallorcine, F
2017/04/25 10:35:30	47.197	7.451	601/227	4	2.8	2.9	A	Grenchen, SO ( <i>GRE</i> )
2017/05/13 00:49:46	46.489	7.102	574/149	4	2.7	2.7	A	Château-d'Oex, VD
2017/06/02 19:05:13	46.267	7.300	589/124	7	3.3	3.1	A	Daillon, VS ( <i>DAI</i> )
2017/06/06 07:18:03	46.727	7.233	584/175	5	3.3	3.1	B	St. Silvester, FR ( <i>STS</i> )
2017/07/01 08:10:34	46.491	7.097	574/149	4	4.3	3.9	A	Château-d'Oex, VD ( <i>CDO</i> )
2017/07/01 09:29:54	46.488	7.096	574/149	5	2.6	2.7	A	Château-d'Oex, VD
2017/07/08 00:18:19	46.485	7.103	574/148	4	2.7	2.7	A	Château-d'Oex, VD
2017/09/03 09:15:47	45.726	10.629	999/999	4	3.4	3.3	B	Lago di Garda, I
2017/09/14 19:16:45	46.486	7.104	574/148	5	2.5	2.6	A	Château-d'Oex, VD
2017/09/16 10:28:40	47.282	6.648	540/237	0	2.5	2.5	B	Belleherbe, F*
2017/09/20 01:43:49	46.798	9.059	724/184	7	2.5	2.5	A	Breil/Brigels, GR ( <i>BRI</i> )
2017/10/03 15:16:25	46.340	8.542	685/133	9	2.5	2.3	B	Bosco Gurin, TI
2017/11/02 14:09:09	46.332	7.527	607/131	4	3.1	3.0	A	Crans, VS, ( <i>CRA</i> )
2017/11/03 18:04:33	46.264	7.402	597/124	8	2.8	2.7	A	St-Léonard, VS ( <i>STL</i> )
2017/11/21 09:22:02	47.145	8.546	684/222	32	3.3	3.0	A	Zug, ZG ( <i>ZUG</i> )
2017/12/15 17:37:05	47.630	9.049	721/277	13	2.7	2.5	A	Raperswilen, TG ( <i>RAW</i> )
2018/01/02 11:16:14	46.107	6.875	556/106	8	2.7	2.5	A	Mont Ruan, F ( <i>MRU</i> )
2018/01/08 08:18:49	46.884	10.087	802/196	10	2.7	2.7	B	Silvretthorn, A ( <i>SIH</i> )
2018/01/14 22:57:15	46.328	7.398	597/131	4	2.6	2.5	A	Anzère, VS ( <i>ANZ</i> )
2018/01/17 19:07:19	47.145	9.988	793/225	1	4.1	3.9	B	Klostertal, A ( <i>KLT</i> )
2018/02/01 01:47:33	47.153	9.996	794/226	1	4.1	3.8	B	Klostertal, A ( <i>KLT</i> )
2018/02/20 19:18:18	46.542	10.484	834/159	10	2.5	2.5	A	Stilfserjoch, I ( <i>STJ</i> )
2018/02/24 16:05:26	46.185	7.088	573/115	6	2.6	2.6	A	Dent de Morcles, VS ( <i>DDM</i> )
2018/03/11 23:29:23	47.672	8.014	643/280	17	3.1	2.6	A	Herrischried, D ( <i>HER</i> )
2018/04/08 21:50:18	46.461	7.142	577/146	5	2.9	2.9	A	Château-d'Oex, VD ( <i>CDO</i> )
2018/04/12 02:23:59	47.154	10.010	795/226	0	3.2	3.1	B	Klostertal, A ( <i>KLT</i> )
2018/04/25 17:29:33	46.642	10.488	833/170	12	2.7	2.6	A	Taufers, I
2018/05/04 21:36:42	47.767	7.519	606/291	15	3.3	3.0	A	Rhinegraben, F/D ( <i>RIG</i> )
2018/05/15 15:30:20	46.516	6.869	556/152	2	3.1	3.2	B	Chatel-St-Denis, FR ( <i>CSD</i> )
2018/05/16 09:32:38	46.516	6.867	556/152	1	2.9	2.9	B	Chatel-St-Denis, FR
2018/07/20 22:20:36	46.009	7.860	633/095	6	2.6	2.5	B	Rimpfischhorn, VS ( <i>RIH</i> )
2018/08/16 09:45:11	46.815	10.090	802/188	6	2.8	2.9	B	Val Lavinuoz, GR ( <i>VLV</i> )
2018/08/23 00:09:10	46.187	7.084	573/115	6	3.2	3.0	A	Dent de Morcles, VS ( <i>DDM</i> )
2018/08/30 12:27:40	46.914	8.927	713/197	5	2.8	2.7	A	Urnerboden, UR ( <i>URB</i> )
2018/09/13 08:47:15	46.556	9.809	782/159	4	2.6	2.9	B	Val Bever, GR
2018/09/29 06:31:03	46.369	6.490	527/136	0	2.6	2.6	B	Thonon-les-Bains, F
2018/11/03 00:20:06	46.079	7.097	574/103	9	2.9	2.7	A	Martigny, VS ( <i>MAR</i> )
2018/11/23 00:52:08	46.262	7.403	597/123	8	2.5	2.3	A	St-Léonard, VS ( <i>STL</i> )
2018/12/15 00:21:09	45.982	7.926	638/092	7	2.5	2.4	A	Cima di Jazzi, I ( <i>CDJ</i> )
2018/12/15 18:12:48	46.341	7.574	610/132	9	2.5	2.4	A	Salgesch, VS ( <i>SAL</i> )
2018/12/29 08:29:36	46.825	7.199	582/186	6	2.9	2.6	A	Fribourg, FR ( <i>FRI</i> )

The values listed under  $M_{WSPEC}$  are the moment magnitudes calculated from the spectral fitting method documented in Edwards et al. (2010). The quality rating (Q) is defined in Table 2. Italicized three-letter abbreviations in the last column correspond to labels used for focal mechanisms in Figs. 2, 4, 5, 6, 7 and Additional file 1: Table S4

\* Based on signal characteristic, we interpret this as an earthquake. However, we cannot entirely rule out the possibility that the signal is associated with a blast due to its shallow source and the proximity to a quarry

**Table 2 Criteria and location uncertainty corresponding to the quality rating (Q) of the hypocentral parameters in the event list in Table 1**

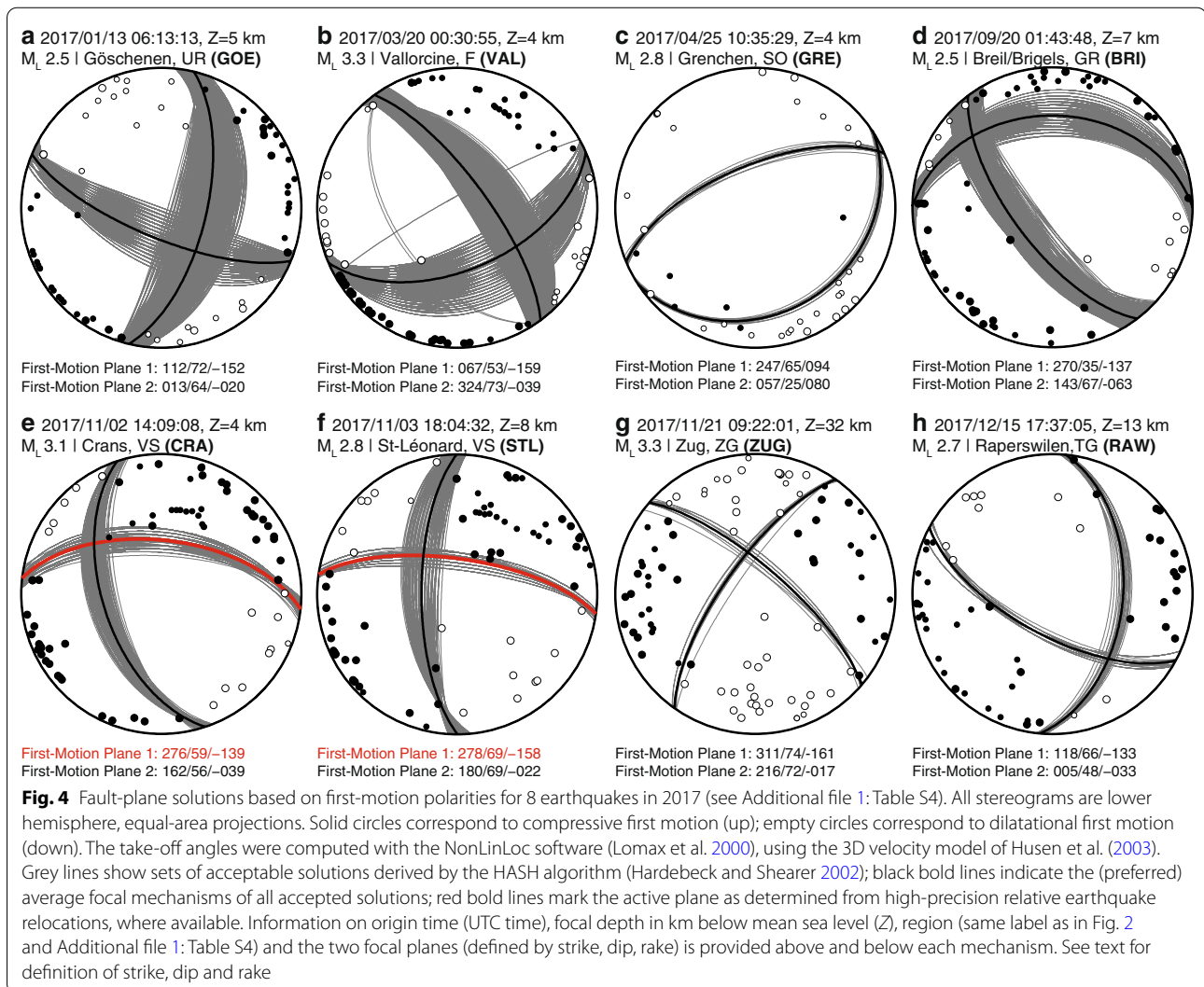
Rating	Criteria		Uncertainty	
	GAP (degrees)	DM (km)	H (km)	Z (km)
A	≤ 180	≤ 1.5 × Z	≤ 2	≤ 3
B	≤ 200	≤ 25	≤ 5	≤ 10
C	≤ 270	≤ 60	≤ 10	> 10
D	> 270	> 60	> 10	> 10

GAP largest angle between epicentre and two adjacent stations, DM minimum epicentral distance, H horizontal location, Z focal depth

this report. The strike angle of a fault plane is measured clockwise from north, with the fault dipping down to the right of the strike direction. The dip angle of the fault plane is measured downward from the horizontal. The

slip direction is defined by the rake angle, which indicates the angle between the slip direction and the strike of the fault plane as measured within the fault plane. Six events in 2017/18 generated sufficient long-period energy to produce a high-quality full-waveform moment-tensor inversion (Figs. 5 and 6). Moment magnitudes derived from this procedure range between  $M_W$  3.1 and  $M_W$  4.1. Additional  $M_W$  values derived from the spectral fitting method of Edwards et al. (2010) are listed in Table 1.

Figure 8 shows the epicentres of the 1032 earthquakes with  $M_L \geq 2.5$ , which have been recorded in Switzerland and surrounding regions over the period 1975–2018. The number of earthquakes with  $M_L \geq 2.5$  between 1975 and 2018 accounts for about 6% of the total number of events detected during that time in the same area. The majority of earthquakes with  $M_L \geq 2.5$  in 2017/18 occurred in regions that have been seismically active in previous years (Fig. 8). In the following section we discuss



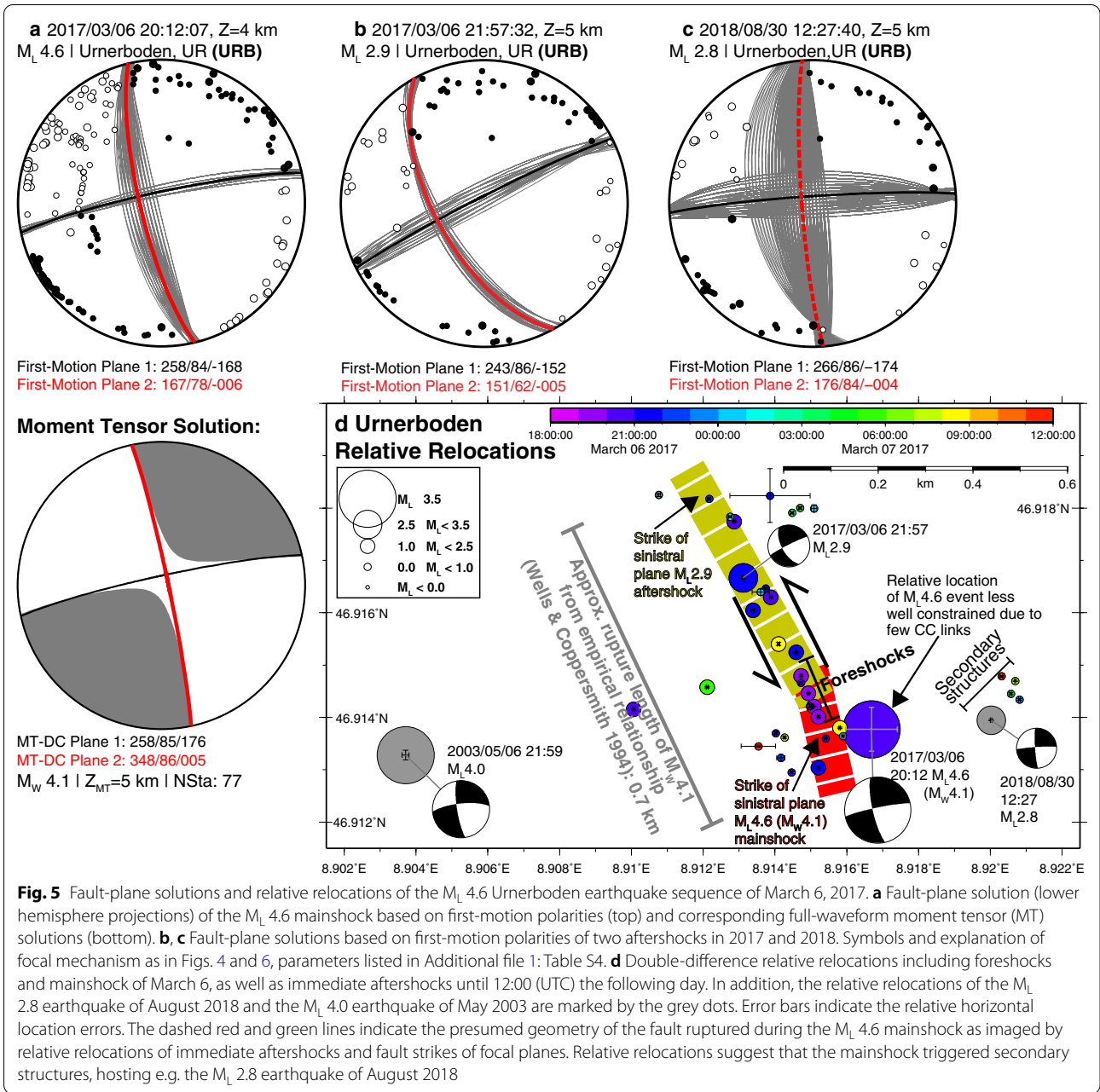


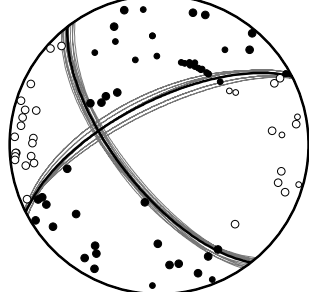
**Fig. 5** Fault-plane solutions and relative relocations of the  $M_L$  4.6 Urnerboden earthquake sequence of March 6, 2017. **a** Fault-plane solution (lower hemisphere projections) of the  $M_L$  4.6 mainshock based on first-motion polarities (top) and corresponding full-waveform moment tensor (MT) solutions (bottom). **b, c** Fault-plane solutions based on first-motion polarities of two aftershocks in 2017 and 2018. Symbols and explanation of focal mechanism as in Figs. 4 and 6, parameters listed in Additional file 1: Table S4. **d** Double-difference relative relocations including foreshocks and mainshock of March 6, as well as immediate aftershocks until 12:00 (UTC) the following day. In addition, the relative relocations of the  $M_L$  2.8 earthquake of August 2018 and the  $M_L$  4.0 earthquake of May 2003 are marked by the grey dots. Error bars indicate the relative horizontal location errors. The dashed red and green lines indicate the presumed geometry of the fault ruptured during the  $M_L$  4.6 mainshock as imaged by relative relocations of immediate aftershocks and fault strikes of focal planes. Relative relocations suggest that the mainshock triggered secondary structures, hosting e.g. the  $M_L$  2.8 earthquake of August 2018

(See figure on next page.)

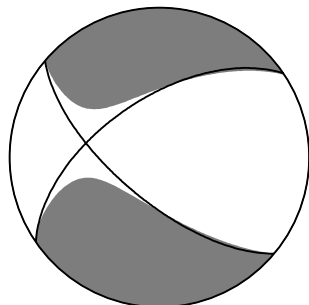
**Fig. 6** Lower hemisphere projections of first-motion fault-plane solutions (top row) and corresponding full-waveform moment tensor (MT) solutions (bottom row) for 6 earthquakes in 2017 and 2018 (see Additional file 1: Table S4). Symbols and explanation of first-motion mechanism as in Fig. 4. Black bold lines on the moment tensor indicate the double-couple part of the MT solution. Red bold lines on the MT solution mark the active plane as determined from high-precision relative earthquake relocations. Strike/Dip/Rake of the double-couple part of the MT (MT-DC) as well as the associated moment magnitude ( $M_w$ ) are provided below the MT solution. No MT solution is available for the  $M_L$  4.1 Klostertal earthquake of January 2018 (**d**)



**a** 2017/06/02 19:05:12, Z=7 km  
M<sub>L</sub> 3.3 | Daillon, VS (DAI)

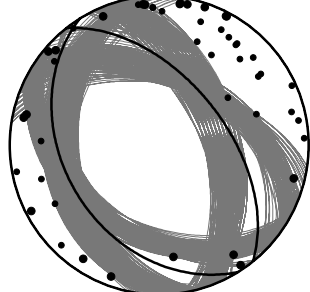


First-Motion Plane 1: 243/67/-154  
First-Motion Plane 2: 142/66/-025

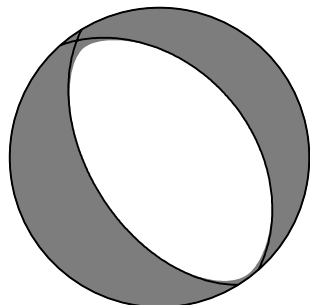


MT-DC Plane 1: 236/58/-152  
MT-DC Plane 2: 130/67/-035  
M<sub>W</sub> 3.2 | Z<sub>M1</sub>=5 km | NSta: 11

**b** 2017/06/06 07:18:03, Z=5 km  
M<sub>L</sub> 3.3 | St. Silvester, FR (STS)

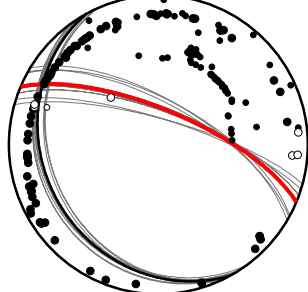


First-Motion Plane 1: 148/36/-084  
First-Motion Plane 2: 321/54/-094

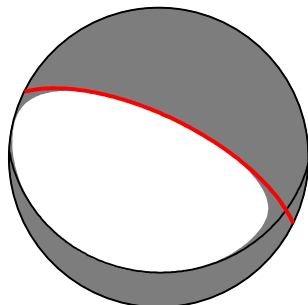


MT-DC Plane 1: 149/51/-084  
MT-DC Plane 2: 319/39/-098  
M<sub>W</sub> 3.2 | Z<sub>M1</sub>=5 km | NSta: 16

**c** 2017/07/01 08:10:34, Z=4 km  
M<sub>L</sub> 4.3 | Chateau-D'Oex, VD (CDO)

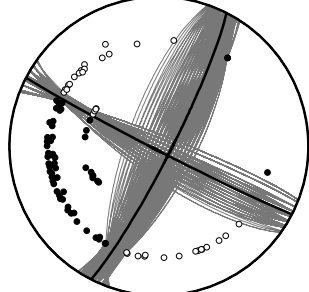


First-Motion Plane 1: 293/71/-105  
First-Motion Plane 2: 153/24/-053



MT-DC Plane 1: 296/68/-081  
MT-DC Plane 2: 092/24/-112  
M<sub>W</sub> 4.0 | Z<sub>M1</sub>=5 km | NSta: 79

**d** 2018/01/17 19:07:19, Z=1 km  
M<sub>L</sub> 4.1 | Klostertal, A (KLT)

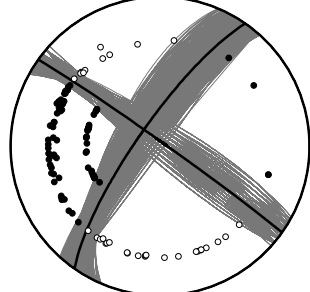


First-Motion Plane 1: 117/88/-173  
First-Motion Plane 2: 027/83/-002

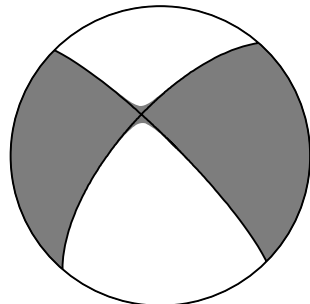


MT-DC Plane 1: 315/81/-157  
MT-DC Plane 2: 221/67/-010  
M<sub>W</sub> 3.8 | Z<sub>M1</sub>=5 km | NSta: 29

**e** 2018/02/01 01:47:33, Z=1 km  
M<sub>L</sub> 4.1 | Klostertal, A (KLT)

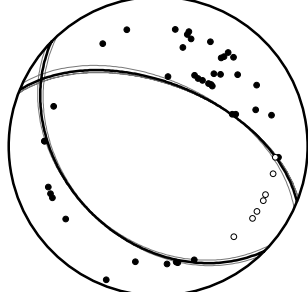


First-Motion Plane 1: 305/88/-168  
First-Motion Plane 2: 215/78/-002

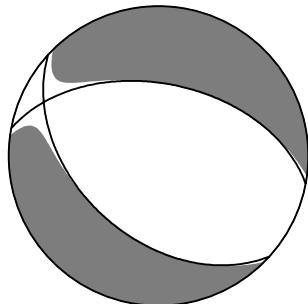


MT-DC Plane 1: 315/81/-157  
MT-DC Plane 2: 221/67/-010  
M<sub>W</sub> 3.8 | Z<sub>M1</sub>=5 km | NSta: 29

**f** 2018/05/15 15:30:20, Z=2 km  
M<sub>L</sub> 3.1 | Chatel-St-Denis, FR (CSD)



First-Motion Plane 1: 134/37/-072  
First-Motion Plane 2: 292/55/-103



MT-DC Plane 1: 132/45/-066  
MT-DC Plane 2: 281/50/-112  
M<sub>W</sub> 3.1 | Z<sub>M1</sub>=5 km | NSta: 9

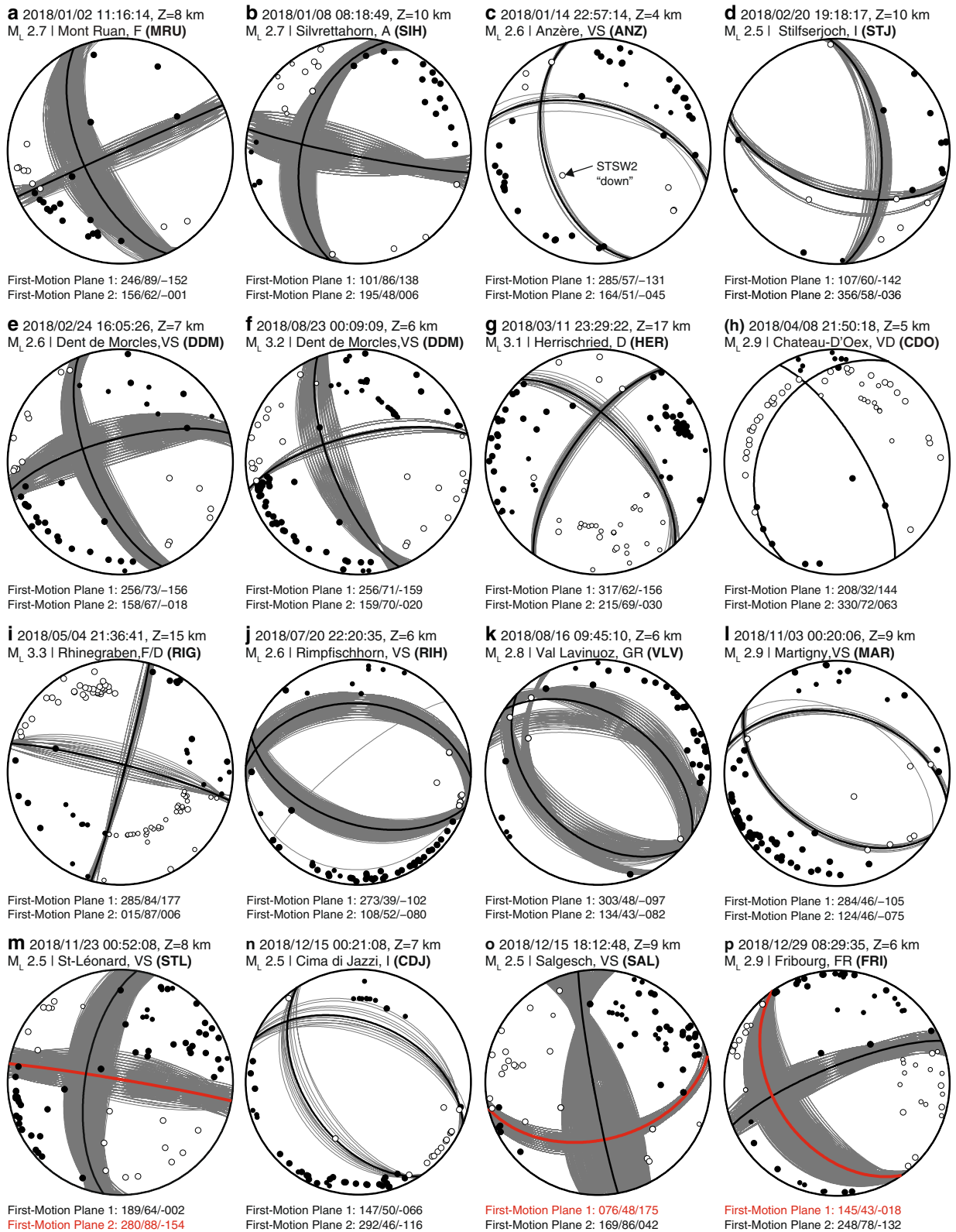
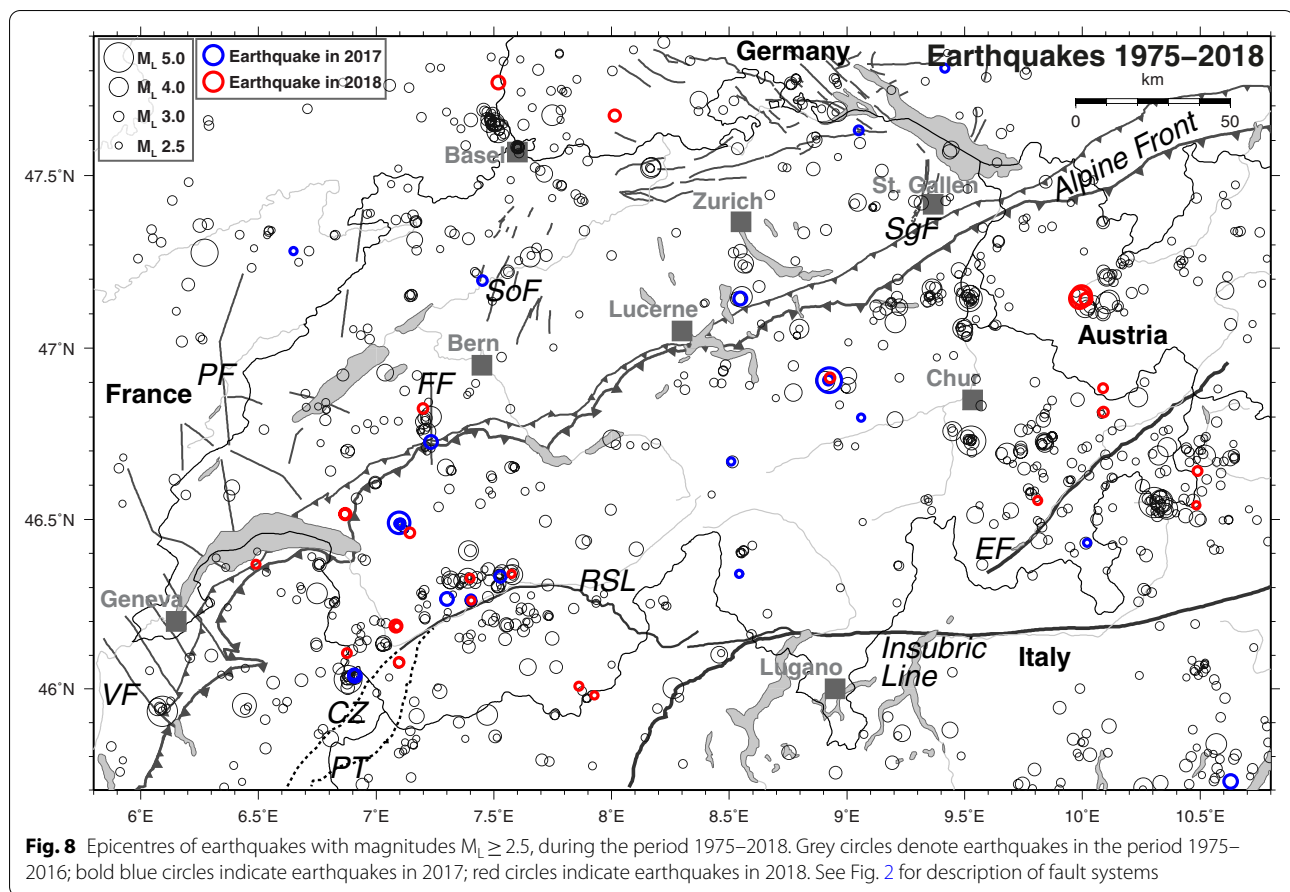


**Fig. 7** Fault-plane solutions (lower hemisphere projections) based on first-motion polarities for 16 earthquakes in 2018 (see Additional file 1: Table S4). Symbols and explanation as in Fig. 4



significant and noteworthy earthquakes and earthquake sequences for the period 2017/18.

### 3.2 Discussion of noteworthy earthquakes in 2017

#### 3.2.1 Göschenen (UR)

On January 13 2017, an  $M_L$  2.5 earthquake occurred about 6 km west of Göschenen (UR) (GOE, Fig. 2a). It is located within a cluster of earthquakes that has been active since at least 2011 and contains a total of 45 events detected and located by the end of 2018. The focal mechanism derived for this event indicates dominantly strike-slip faulting with a small normal-fault component (Fig. 4a). The mechanism is virtually identical to the mechanism of an  $M_L$  3.2 earthquake of the same cluster, which occurred in October 2016 (Diehl et al. 2018). The focal depth derived with SED's routine velocity model of Husen et al. (2003) is about 5 km. With a distance to the closest station of about 14 km, we estimate the uncertainty of the focal depth to be in the order of  $\pm 2$  km. Despite this uncertainty, the earthquake certainly locates within the crystalline Aar Massif and the ongoing seismic activity suggests active strike-slip deformation in

the internal part of the massif, possibly along reactivated WNW–ESE striking shear-zones (see Diehl et al. 2018).

#### 3.2.2 Urnerboden (UR/SZ)

With a magnitude of  $M_L$  4.6, the largest event in the reporting period occurred 1–2 km north of the Urnerboden valley in the border region of canton Uri, Schwyz and Glarus on March 6, 2017 (URB, Fig. 2a). This event also represents the strongest earthquake within Switzerland since the  $M_L$  5.0 Vaz earthquake of 1991 and has the seventh largest magnitude of all earthquakes instrumentally located by the SED within the geographic boundaries of Fig. 2 since 1984. The mainshock occurred at 20:12 (UTC) at a depth of about 4 km and it was felt by large parts of the population in eastern and central Switzerland (Fig. 9a). The maps in Fig. 9 show the spatial distribution of the interpolated macroseismic intensity (see Sect. 2.3), along with observed macroseismic intensities based on felt reports from online questionnaires. The felt reports shown in the maps are aggregated by postal code. We show only reports with associated quality levels “good” or higher (i.e., based on more than eight



consistent reports from a postal code area) to minimize possible bias induced by using automatically processed questionnaires. The final macroseismic field depicted in the ShakeMap of Fig. 9a is the result of a weighted average of the converted predicted ground-motions and the station recordings. Colours in Fig. 9a are proportional to macroseismic intensity levels according to the European Macroseismic Scale (EMS-98; Grünthal 1998) and indicate that the largest intensities well constrained by felt reports are of degree V. The interpolated ShakeMap intensities in Fig. 9a suggest that intensity may have approached degree VI in the alluvium-filled Linth valley, a few km east of the earthquake epicentre. A degree VI intensity, however, would imply cases of slight damage for masonry building types such as hair-line cracks or falling of small pieces of plaster (Grünthal 1998). The SED received only two reports indicating such damages in a distance of about 20 km from the epicentre. Due to the low number of unconfirmed damages reported to the SED, it remains questionable if a degree VI was actually observed. The lack of degree VI observations might also be due to the fact that the epicentre locates in a remote area. If such an event occurs in a densely settled area, a considerable number of cases of small damage would be likely.

With  $85 \text{ cm/s}^2$ , the highest acceleration associated with the Urnerboden earthquake is measured at station SLTM2 at a distance of about 6 km from the epicentre (Fig. 10). Station SLTM2 is located on rockslide deposits in the centre of a small Alpine valley in Linthal village. The peak ground velocity at the same station reached  $2 \text{ cm/s}$  (Fig. 10), consistent with macroseismic intensity levels exceeding degree V in the epicentral area (Faenza and Michélini 2010). The shaking levels are remarkably lower ( $10 \text{ cm/s}^2$ ) at station LLS (Fig. 10), at comparable distance from the earthquake epicentre, but located on very hard rock in Linth–Limmern. The ground shaking amplitudes ( $29 \text{ cm/s}^2$ ) and duration increase again at station SALTS (Altdorf-Hospital; Fig. 10) located at 22 km from the epicentre on an alluvial fan at the edge of the Reuss alluvial plain. Both SLTM2 and SALTS exhibit an amplification of about 2 over a broad frequency range compared to the Swiss reference model of Edwards and Fäh (2013), while LLS is known to show analogous de-amplification (see Michel et al. 2014 and stations.seismo.ethz.ch). The amplification effects shown in Fig. 10 document the severe impact of local site effects on the ground shaking for such earthquakes.

With the closest station at 6 km distance, the focal depth of about 4 km is relatively well constrained and we estimate its uncertainty to be in the order of  $\pm 1 \text{ km}$ . The mainshock was preceded by a sequence of at least 6 foreshocks of magnitudes ranging between  $M_L$  0.5 and

2.2. The first detected and located event of this foreshock sequence occurred at 19:40 (UTC), about 32 min before the mainshock. To improve the location quality of aftershocks, two temporary stations were immediately deployed in the epicentre region. The first station (URN1) was installed in the Urnerboden valley, about 1.5 km south of the epicentre on March 7. The following day, a second station (URN2) was installed south of Bisisthal (SZ), about 6 km WNW of the epicentre region. Both stations were in operation through July 11, 2017. To lower the completeness magnitude of the aftershock sequence, standard detections were complemented by template-matching detections (see Sect. 2.3) at station PANIX. For the first 17 days of the aftershock sequence, all template matching detections missed by the SED standard procedures have been reviewed and, if possible, manually located. During the first two weeks following the mainshock, 67 aftershocks with  $M_L$  ranging between  $-0.1$  and  $2.9$  have been located by the SED. The largest aftershock of  $M_L$  2.9 took place about 1 h and 45 min after the  $M_L$  4.6 mainshock and on August 30, 2018, about 18 months after the mainshock, an  $M_L$  2.8 earthquake occurred in the aftershock region.

The fault plane solution derived for the  $M_L$  4.6 mainshock is very close to a pure strike-slip mechanism (Fig. 5a top, Additional file 1: Table S4). The corresponding moment tensor solution differs only slightly from the first-motion solution (Fig. 5a bottom), differences are within the uncertainty in the dip of the NNW–SSE striking plane of the first-motion solution. The moment magnitude derived from the full-waveform inversion is  $M_W$  4.1. Although the difference of 0.5 between  $M_L$  and  $M_W$  deviates from the average 0.3 difference predicted by the scaling-relationship of Goertz-Allmann et al. (2011) for this magnitude range, it is still within the uncertainty of this relationship ( $\sigma_{M_W} \pm 0.2$ ). As discussed later in more detail, the focal mechanism of the immediate  $M_L$  2.9 aftershock of March 6 shows differences in strike compared to the mainshock (Fig. 5b). The mechanism of the  $M_L$  2.8 event of August 2018 (Fig. 5c) indicates a strike-slip rupture similar to the mainshock, however, uncertainties are larger.

Figure 5d shows the relative relocations of fore-, main- and immediate aftershocks through March 7, 12:00 (UTC). We also included an  $M_L$  2.8 event of August 2018 and an  $M_L$  4.0 event of May 2003 in the double-difference relative relocation (see Fig. 5d). As indicated by the error bars in Fig. 5d, uncertainties of the relative location of the  $M_L$  4.6 mainshock are higher due to the low degree in waveform similarity between mainshock and the majority of smaller fore- and aftershocks. This effect is related to differences in the frequency content of the signals (e.g., Bachura and Fischer 2019) and leads to a low

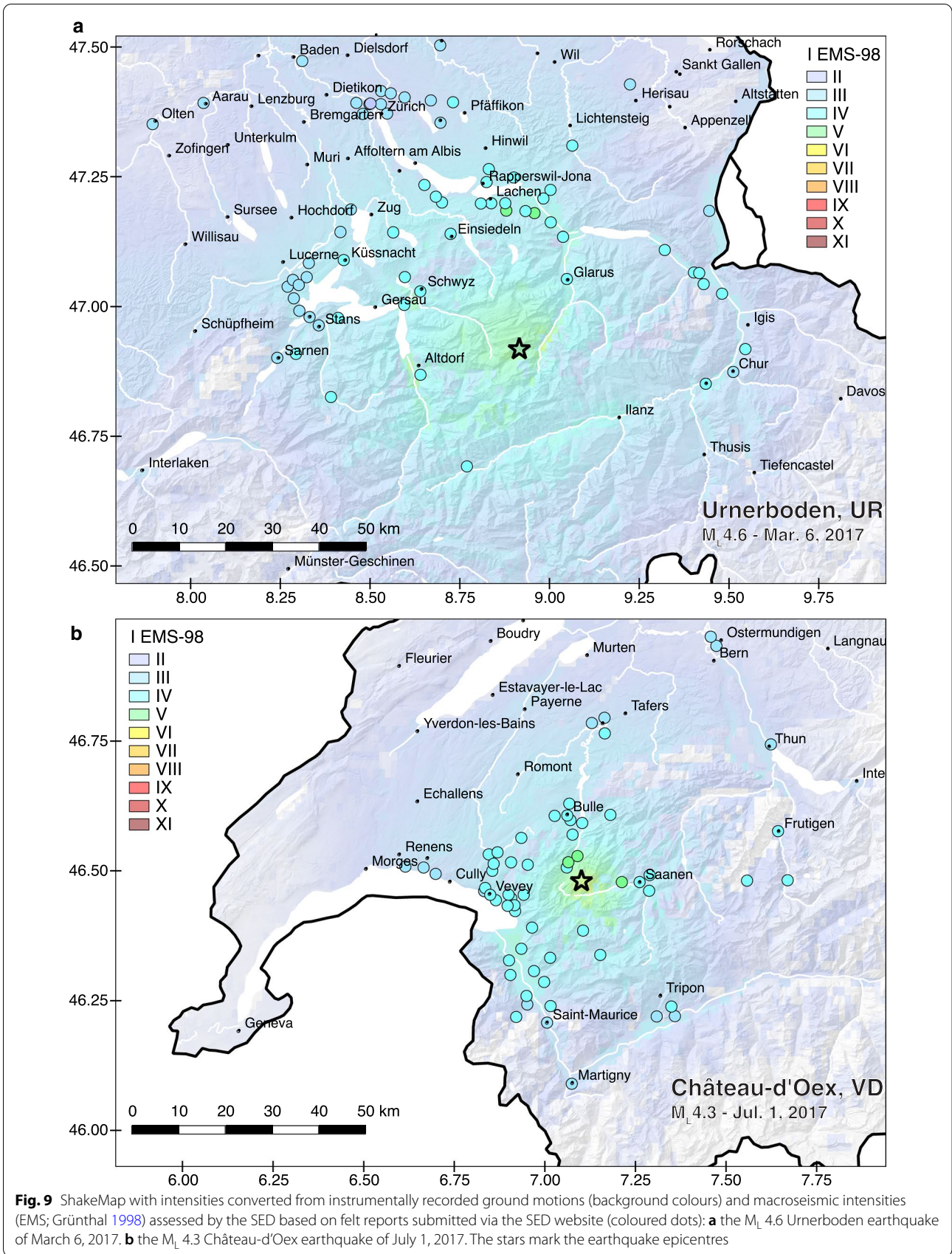


**Fig. 9** ShakeMap with intensities converted from instrumentally recorded ground motions (background colours) and macroseismic intensities (EMS; Grünthal 1998) assessed by the SED based on felt reports submitted via the SED website (coloured dots): **a** the M<sub>L</sub> 4.6 Urnerboden earthquake of March 6, 2017. **b** the M<sub>L</sub> 4.3 Château-d'Oex earthquake of July 1, 2017. The stars mark the earthquake epicentres

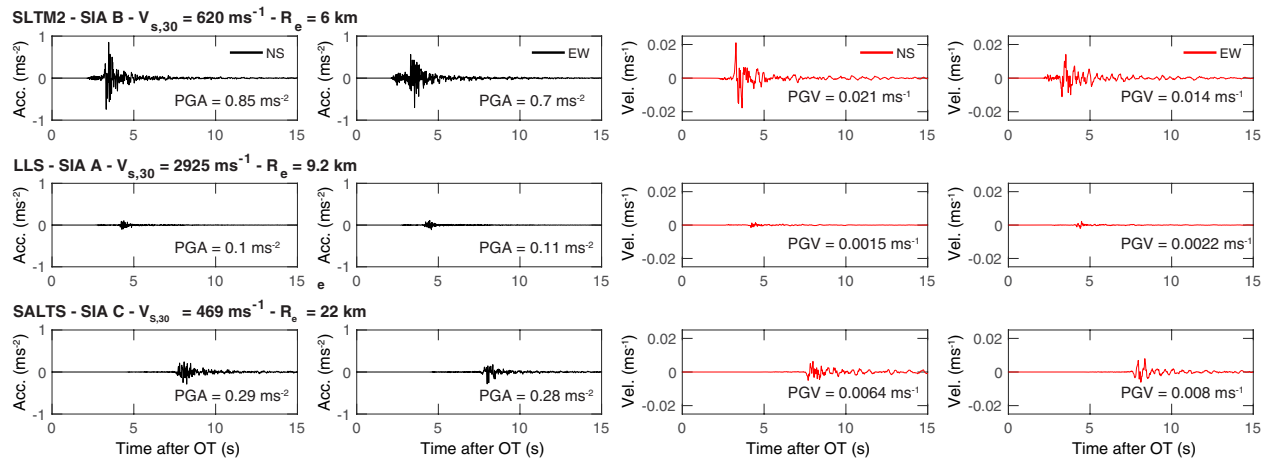


**Fig. 10** Ground acceleration (left panels, black seismograms) and velocity (right panels, red seismograms) as recorded at three selected strong-motion stations located within 25 km of the epicentre of the  $M_L$  4.6 Urnerboden earthquake of March 6, 2017. The data are restituted (corrected to account for the instrumental response) to ground motions and filtered with an acausal bandpass filter between 0.3 Hz and 80% of the Nyquist frequency (for details see Cauzzi et al. 2016). Site class (SIA), shallow shear-wave  $V_{s,30}$  and epicentral distance ( $R_e$ ) are indicated for each station

number of cross-correlation measurements and therefore weaker linkage between the mainshock with the rest of the sequence. We therefore interpret the eastward offset of about 100 m of the mainshock from the main lineament of fore- and immediate aftershocks as an artefact. The fact that the formal error bars of the mainshock approach the foreshock region (Fig. 5d) suggests that the mainshock actually locates on the main lineament. In addition, the proximity between foreshocks and mainshock (Fig. 5d) indicates a nucleation phase in advance of the mainshock. We estimate a rupture length of about 0.6 km for the  $M_L$  4.6 mainshock from the extent of relocated fore- and immediate aftershocks (proposed rupture plane indicated by red and green dashed lines in Fig. 5d). This estimate is in good agreement with a rupture length of 0.7 km derived from empirical relationships (Wells and Coppersmith 1994) for an  $M_w$  4.1 strike-slip earthquake. In combination with the focal mechanisms from the two events on March 6 (Fig. 5a, b), the relative relocations indicate a sinistral rupture on a NNW–SSE striking plane. However, the geometry of the relocations together with a well resolved difference of about  $16^\circ$  in strike of the sinistral focal plane between the mainshock (strike:  $167^\circ$ ; red dashed line in Fig. 5d) and the  $M_L$  2.9 aftershock (strike:  $151^\circ$ ; red dashed line in Fig. 5d) suggest a westward bend or jog along the rupture plane. Alternatively, the rupture might have extended over two or more fault segments of variable orientation (e.g. Riedel shears), which are expected to exist in a complex and fractured strike-slip system. Evidence for the existence of such a fractured fault system is provided by the spread in

locations in Fig. 5d, indicating the triggering of off-fault structures by the mainshock. A prominent example is the event of August 2018. Although the focal mechanism is very similar to the one of the mainshock, its location is clearly separated from the  $M_L$  4.6 rupture. Additional evidence for the existence of a system of strike-slip faults in this area is provided by the  $M_L$  4.0 Urnerboden earthquake of May 6, 2003 (Deichmann et al. 2004). Although its strike-slip focal mechanism is virtually identical to the  $M_L$  4.6 mainshock of 2017 (see Fig. 5d), relative relocations combining both sequences confirm that the event of 2003 locates about 1 km west of the sequence of 2017 and therefore occurred on a sub-parallel fault (Fig. 5d).

The base of the autochthonous Mesozoic units in this part of the Helvetic nappes is estimated to lie at a depth of about 1.5 km (Pfiffner 2014). We therefore conclude that, with a focal depth of 4 km (with the estimated uncertainty of about  $\pm 1$  km), the source is probably located within the uppermost parts of the crystalline Aar Massif. Together with previous events like the  $M_L$  3.8 Linthal earthquake of 2001 (Deichmann et al. 2002) and the 2003  $M_L$  4.0 Urnerboden earthquake, both located at a similar depth (about 3 km) and of almost identical focal mechanisms, the  $M_L$  4.6 Urnerboden earthquake of 2017 documents ongoing strike-slip deformation in the top part of the eastern Aar Massif. The stress field indicated by the P-axis (maximum principal stress) and T-axes (minimum principal stress) of these earthquakes is approximately consistent with the strike-slip regime proposed by Marschall et al. (2013) for the Helvetic domain in eastern Switzerland, with sub-horizontal P-axis in NW–SE



direction and sub-horizontal T-axis in NE–SW direction. In principle, this strike-slip regime is also consistent with the mechanism derived for the Göschenen event of 2017 (Fig. 4a) discussed in the previous section. Orientations of P and T-axis, however, seem to be rotated about 30° clockwise compared to the Urnerboden earthquake, indicating possible second-order variations of the stress regime or local stress variations on pre-existing faults along-strike of the Aar Massif.

### 3.2.3 Vallorcine (France)

The  $M_L$  3.3 and  $M_L$  3.0 earthquakes of March 20, 2017 (VAL, Fig. 2a) are part of the on-going earthquake sequence that followed the  $M_L$  4.9 earthquake of September 2005 (e.g., Deichmann et al. 2006; Fréchet et al. 2010; Diehl et al. 2013, 2015, 2018; Cara et al. 2017). Both events on March 20 were felt by the local population and intensities reached degree IV. The focal depths of 4 km are well resolved by P and S phases observed at station SEMOS located in a distance of about 4 km from the epicentre. Focal depths and the strike-slip fault plane solution of the  $M_L$  3.3 earthquake (Fig. 4b) are very similar to past events of this sequence.

### 3.2.4 Grenchen (SO)

On April 25, 2017, an  $M_L$  2.8 earthquake occurred about 4 km east to the town of Grenchen (SO) (GRE, Fig. 2a). With an intensity of degree IV, it was felt by the local population and the hypocentre derived with SED's standard velocity model of Husen et al. (2003) indicates a shallow source at a depth of about 4 km. With phases observed at the two SSMNet stations in Solothurn (SOLZ, SOLB), which are located at epicentral distances of 5 and 7 km, the formal uncertainty of the focal depth is about  $\pm 2$  km. However, errors in the standard velocity model, especially for S-waves in the foreland, are expected and result in possibly even larger uncertainties. Strong surface waves similar to quarry-blast signals as well as hypocentre solutions computed with alternative P- and S-wave velocity models suggest an even shallower source close to the surface, at depths between 0 and 2 km. Within a distance of about 4 km, two similarly shallow  $M_L$  2.7 events occurred in October 1993 that might be associated with the same structure. The first-motion focal mechanism derived for the Grenchen event of 2017 (Fig. 4c) indicates reverse faulting. Since we consider it mechanically unlikely that the steep (65°), NW dipping plane was activated in reverse sense, we interpret the shallower plane dipping about 25° towards SE as the active fault plane. The event locates at the northern boundary of the Molasse basin (also referred to as "subjurassic zone", e.g., Mock and Herwegh 2017), straddling the southern foothills of the Jura mountains between the Weissenstein- and

Arch-Anticline (e.g., Meier 2010). The base of the Mesozoic sediments in the epicentral region lies at a depth of about 1.5–2 km and the vertical thickness of the Mesozoic units is about 1.5 km (e.g., Sommaruga et al. 2012; Mock and Herwegh 2017). If located in the sedimentary cover, as suggested by the waveforms, the source is likely within the Mesozoic units. In this case, the SE-dipping, low-angle thrust fault might be associated with the main basal Jura décollement or a secondary thrust, located above the main décollement level. A source in the sedimentary cover would be indicative for possible ongoing thin-skinned deformation. However, considering the current hypocentre uncertainties, we cannot rule out a source in the pre-Mesozoic Permo-Carboniferous trough or Variscan basement. In any case, the Grenchen earthquake of 2017, together with the earthquake sequence of the year 2000 near Saint Ursanne (Lanza et al. 2019, 2020), represents a rare example of shallow thrust faulting in the vicinity of the Jura fold-and-thrust belt, indicating seismically active contraction in the northwestern Alpine foreland of Switzerland.

### 3.2.5 Dailion (VS)

The  $M_L$  3.3 Dailion earthquake (DAI, Fig. 2a) occurred about 6 km NW of Sion at 19:05 (UTC) on June 2, 2017. With more than 400 felt reports received by the SED, this event was strongly perceived by the population in the Valais and the maximum intensity reached degree IV. The focal depth of about 7 km is well resolved by the dense network in the Valais (Fig. 1) and with the closest station at an epicentral distance of about 6 km distance from the epicentre, we estimate the uncertainty to be on the order  $\pm 1$  km. The first-motion mechanism in Fig. 6a (top) is of excellent quality and low signal-to-noise levels allowed the computation of a moment-tensor for this event (Fig. 6a, bottom), with a moment magnitude of  $M_w = 3.2$  and a corresponding focal mechanism similar to the first-motion solution (Fig. 6a). The mechanism suggests strike-slip faulting with a small normal-fault component. The active plane could not be determined due to the lack of aftershocks (only one aftershock was detected). However, the NE–SW striking dextral plane would be consistent with orientation and kinematics of the dextral Rhone-Simplon Line (RSL), which locates about 6 km to the south of the epicentre.

### 3.2.6 St. Silvester (FR)

On June 6, 2017, an  $M_L$  3.3 earthquake occurred close to the village of St. Silvester (STS, Fig. 2a). Reported intensities reached degree IV in the epicentre region and most felt reports (intensity III) were received from the city of Fribourg (about 20 reports), located about 10 km NW of

the epicentre. The source was located at a depth of about 5 km. However, with the closest station located within the Molasse basin at a distance of about 9 km, the absolute uncertainty using SED's standard velocity model is probably on the order of  $\pm 2\text{--}3$  km. Although the focal mechanism computed from first-motion polarities has considerable uncertainties (Fig. 6b, top), the distribution of exclusively compressional (“upward”) polarities can only be explained by a normal-fault mechanism. A normal-fault mechanism is also confirmed by the available moment-tensor solution shown in Fig. 6b (bottom). The corresponding moment magnitude is  $M_w = 3.2$ . The epicentre of the earthquake locates at the southern end of the Fribourg Fault Zone (Fig. 2a; see location of STS), in the subalpine Molasse units, about 1 km north of the front of the Préalpes nappes. In comparison with structural models of Vouillamoz et al. (2017) and Gruber (2017), the focal depth of 5 km suggests a source within the pre-Mesozoic basement. However, due to the depth uncertainties, we cannot entirely rule out a source in the lower Mesozoic units. The event locates within the St. Silvester structure proposed by Vouillamoz et al. (2017). However, its normal-fault mechanism substantially deviates from the N–S oriented sinistral strike-slip regime of the Fribourg Fault. In addition, the earthquake likely occurred in the basement and therefore below the Fribourg Fault, which is assumed to be restricted to the sedimentary cover (e.g., Vouillamoz et al. 2017). The St. Silvester event of 2017 therefore suggests potential structural complexity towards the southern termination of the N–S striking Fribourg Fault. Its normal-fault mechanism is similar to the  $M_L$  3.8 Jaun earthquake of May 1999 (Deichmann et al. 2000) and indicates the transition from N–S oriented sinistral strike-slip faulting along the Fribourg Fault to predominantly NE–SW or NNE–SSW directed normal faulting within the Préalpes domain.

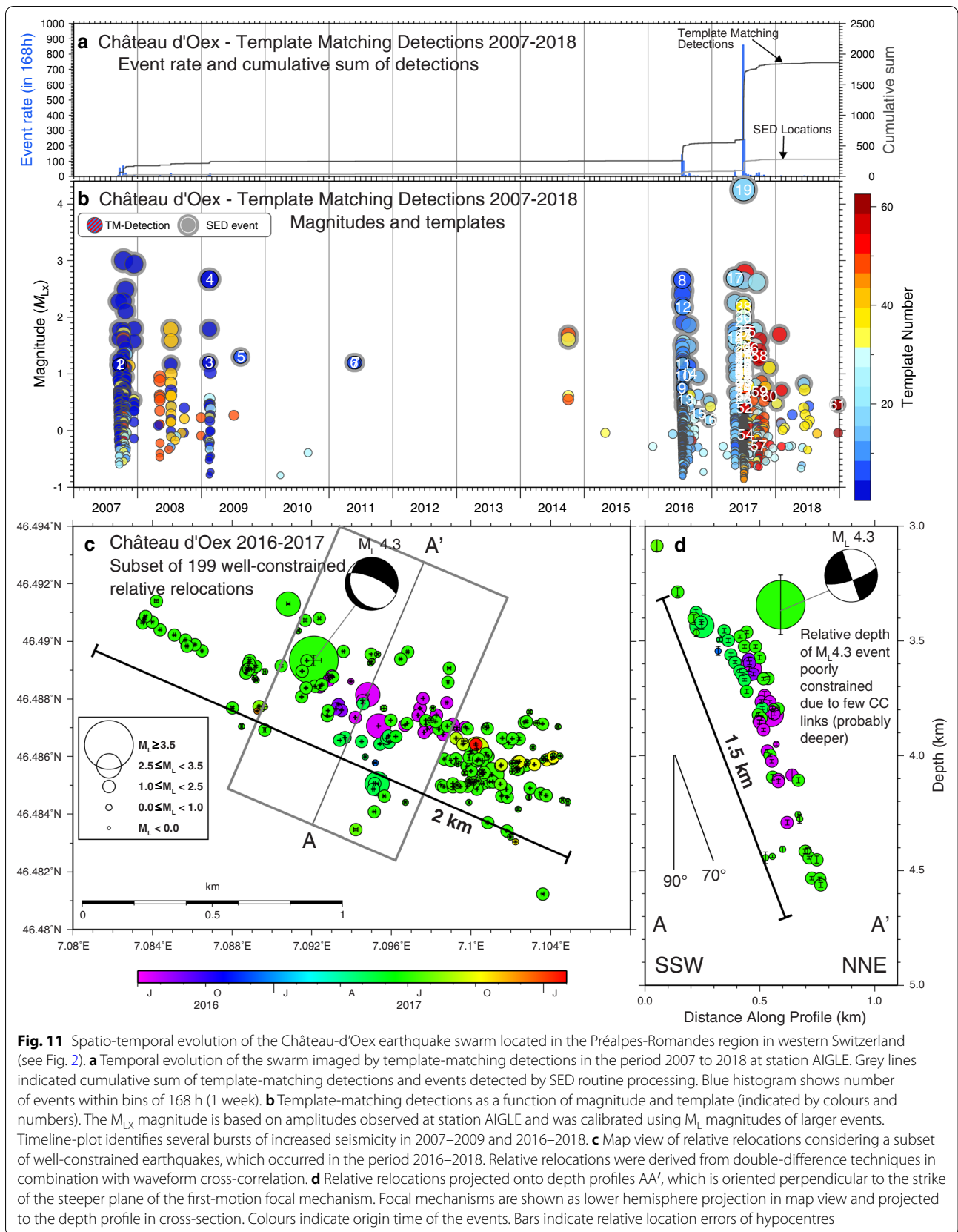
### 3.2.7 Château-d'Oex (VD), 2017

With a magnitude of  $M_L$  4.3, the second largest earthquake in the reporting period occurred close to the town of Château-d'Oex in the Prealps region on July 1, 2017 (CDO, Fig. 2a). The mainshock was felt in large parts of western Switzerland (Fig. 9b), especially in the Molasse basin to the north as well as along the NE coast of Lake Geneva and to its south within the lower Rhone valley. More than 1000 felt reports were received by the SED. Similar to the Urnerboden earthquake, the ShakeMap intensity reached degree VI in the epicentral area (Fig. 9b). However, the maximum macroseismic intensities reported to the SED within a distance of 8 km from the epicentre are of degree V.

The focal depth of 4 km is well constrained by P and S wave arrivals observed at the SSMNet station in

Château-d'Oex (SCOD) at a distance of about 3 km from the epicentre. As discussed already for previously described earthquakes, additional uncertainty is introduced by the velocity model. Therefore, we estimate the uncertainty in focal depth to be in the order of  $\pm 1\text{--}2$  km for this event. This depth is also consistent with solutions derived for an  $M_L$  2.7 and an  $M_L$  2.5 event in July 2016 (Diehl et al. 2018), which are related to the  $M_L$  4.3 event. This  $M_L$  4.3 earthquake is therefore part of a remarkable earthquake sequence, active at least since 2007, as documented by the temporal evolution imaged by template-matching detections in Fig. 11a, b. Between September and December 2007, a sequence of 23 earthquakes with  $M_L$  ranging between 0.7 and 2.6 had occurred in this cluster. Since station SCOD was only installed in April 2016, the focal depth was basically unconstrained and solutions between 0 and 10 km were reported (Deichmann et al. 2008). The similarity of waveforms between the sequence in 2007 and the more recent sequences, as indicated by overlapping template events (overlap in colours) in Fig. 11b, suggests that the sequences 2007–2009 have the same source depth of about 4 km as those in 2016–2018. The burst of activity in 2016 initiated with an  $M_L$  2.7 earthquake on July 16, that was followed by 40 “aftershocks” ( $M_L$  0.5–2.5), detected and located by SED routine procedures. The  $M_L$  4.3 event of July 2017 was preceded by a small sequence, which initiated on May 12 and lasted for about 5 days (12 located events, maximum  $M_L = 2.7$ ). Moreover, two “foreshocks” occurred two days before the  $M_L$  4.3 earthquake of July 1. With about 1000 template-matching detection, the aftershock sequence following the  $M_L$  4.3 earthquake was rather intense (Fig. 11a, b). In the following first 2 weeks, the SED detected and located a subset of 193 aftershocks ( $M_L$  ranging between  $-0.1$  and 2.7) by routine methods. To improve completeness and location quality of aftershocks, three temporary stations (CDO1-3) were deployed in the epicentral region on July 4. Station CDO2-3 operated through November 2017 and station CDO1 through June 2018. The aftershock activity ceased towards the end of 2017.

The first-motion mechanism computed for the  $M_L$  4.3 earthquake of July 2017 is shown along with the derived moment-tensor solution in Fig. 6c. The moment magnitude derived from the full-waveform inversion is  $M_w = 4.0$ . Both solutions in Fig. 6c image a normal-faulting mechanism, with a steeply dipping plane (about  $70^\circ$ ) towards NNE and a plane dipping at a low-angle of about  $20^\circ$  towards SSW. However, second-order differences between the two solutions exist in terms of rake and strike of the second plane. These differences are likely caused by several polarity misfits contained in the first-motion solution. Preliminary tests with an improved



3D velocity model suggest that these misfits are primarily related to errors in take-off angles caused by un-modelled velocity structures in the current SED standard velocity model. Take-off angles computed with the improved model result in a first-motion mechanism similar to the moment-tensor solution of Fig. 6c.

Finally, we performed a double-difference relative relocation of the Château-d'Oex cluster for events that occurred between July 2016 and January 2018. We considered only well locatable events linked to neighbouring events by at least 10 cross-correlation and 10 bulletin-pick differential times. The relative relocations of the resulting 199 events are shown in map view in Fig. 11c and are projected to a vertical profile in Fig. 11d. The vertical profile is oriented perpendicular to the strike of the steeply dipping focal plane (Plane 1 of Fig. 6c). Due to the effects already discussed for the Urnerboden sequence, the relative location of the  $M_L$  4.3 earthquake is less well resolved, especially in focal depth. This is documented by its relatively larger error bar in Fig. 11d and the vertical offset from the main cluster is therefore interpreted as an artefact. The relative relocations in Fig. 11d confirm the plane dipping towards NNE as the active fault plane. In addition, the geometry imaged by the relocations is in good agreement with the steep dip angle of  $70^\circ$  of the focal mechanism. Events related to the sequence in 2016 locate in the centre of the cluster (Fig. 11c, d), while events in 2017 are distributed over the entire rupture plane. This may indicate that the activity in 2016 occurred in the nucleation zone of the future  $M_L$  4.3 rupture.

In order to constrain the lithology of the source region, we consider two geological profiles. The cross-section of Mosar et al. (1996; their Fig. 2a) locates closest to the Château-d'Oex cluster and indicates that the basal thrust of the Préalpes Médiannes lies at a depth of about 1 km and less in the area of the epicentre NW of the Les Millets anticline. Given a focal depth of 4 km ( $\pm 1$ –2 km) the earthquakes therefore locate below the base of the nappes of the Préalpes Médiannes. The profile of Matzenauer (2012), located about 10 km NE from the cluster and projected onto the region of the hypocentre, indicates an about 2 km thick layer of subalpine Molasse below the basal thrust of the Préalpes Médiannes in the projected hypocentre region. The base of the autochthonous Mesozoic cover lies at a depth of about 5 km in this profile. The interpolated top-basement map of Pfiffner (2014), on the other hand, shows a basement high in the region of the Château-d'Oex earthquake cluster, indicating a depth of the base-Mesozoic of only about 3 km. The focal depth of 4 km therefore suggests that the cluster is likely located near the top of the pre-Mesozoic basement. However, assuming a vertical thickness of the autochthonous

Mesozoic cover of 1.5–2 km (Sommaruga et al. 2012), the focal-depth uncertainty of  $\pm 1$ –2 km and the uncertainties related to the top-basement model do not entirely rule out a source within the autochthonous Mesozoic cover. Similar to the St. Silvester earthquake and to the Jaun earthquake sequence of 1999, the  $M_L$  4.3 Château-d'Oex earthquake documents NNE–SSW directed normal faulting in the Préalpes region, likely near the top of the pre-Mesozoic basement.

### 3.2.8 Zug (ZG)

The  $M_L$  3.3 Zug earthquake (ZUG, Fig. 2a) of November 21, 2017 occurred within the lowermost crust within a distance of less than 1 km to the  $M_L$  4.2 earthquake of February 2012 (Diehl et al. 2013; Singer et al. 2014). As typical for deep crustal earthquakes, it was felt by the population within a relatively large radius, and the SED received more than 300 macroseismic felt reports. The derived strike-slip focal mechanism (Fig. 4g) is well constrained and is virtually identical with the one of the  $M_L$  4.2 earthquake of 2012. It is the first event within this cluster since the  $M_L$  4.2 sequence of February 2012 and indicates ongoing activity of this cluster within the lowermost crust.

## 3.3 Discussion of noteworthy earthquakes in 2018

### 3.3.1 Anzère (VS)

On January 14, 2018, an  $M_L$  2.6 earthquake occurred between the village of Anzère and the Wildhorn summit (ANZ, Fig. 2b). This earthquake locates in the centre of the SW–NE striking earthquake lineament north of the Rhone valley, which is one of the most active clusters in the Central Alps (see Figs. 2 and 8). The cluster has been described to be dominated by strike-slip mechanisms (e.g., Maurer et al. 1997), however, the occurrence of additional reverse as well as transtensive mechanisms suggest a rather complex system of en-echelon faults and step-over geometries (e.g., Diehl et al. 2018). The focal depth of the event is about 4 km and the well-constrained focal mechanism indicates transtensive faulting (Fig. 7c). A smaller ( $M_L$  1.8) event occurred at the same location on February 22, with a mechanism similar to the  $M_L$  2.6 earthquake (Fig. 2b and Additional file 1: Figure S1d). The transtensive Anzère mechanisms are strikingly similar to the ones of the Cranssequence (CRA, Figs. 2a and 4e), which is active since at least 2014 (Diehl et al. 2018) and locates about 9 km to the east. The WNW–ESE striking dextral plane, which has been determined to be the active plane in the Cranssequence (Diehl et al. 2018), deviates from the general SW–NE strike of the earthquake lineament (Fig. 2), consistent with an en-echelon arrangement and segmentation of faults north of the Rhone valley.



### 3.3.2 *Klostertal (Vorarlberg, Austria)*

With magnitudes of  $M_L$  4.1, the two largest earthquakes in 2018 took place north of the Klostertal valley (KLT, Fig. 2b), about 12 km east of Bludenz in western Austria. The first event of January 17 was followed by an event of similar magnitude on February 1. Although the epicentre is located about 20 km from the Swiss border, the SED received about 270 macroseismic felt reports for the earthquake in January. Most felt reports were received from Liechtenstein, the Rhine valley east of St. Gallen and the city of St. Gallen. ShakeMap intensities for both  $M_L$  4.1 earthquakes predict degree V in the epicentre region, which is consistent with the intensity of V reported by the Seismological Service of Austria (ZAMG).

With the closest observing station DAVA, located at a distance of about 18 km, the derived depth close to the surface (depth of  $-1$  km, Table 1) is poorly constrained. Hypocentre solutions therefore vary between surface and 10 km depth depending on the selected distance range and phase types. We prefer a shallow source, because this is consistent with the strong surface waves observed in the seismograms. However, the estimated uncertainty in focal depth is in the order of at least  $\pm 5$  km. A first-motion mechanism was derived for the event in January (Fig. 6d), first-motion and moment-tensor solutions are available for the event in February (Fig. 6e). The corresponding moment magnitude is  $M_W=3.8$  and the focal depth of 5 km derived by the moment-tensor inversion provides additional evidence for a shallow source. First-motion and moment-tensor mechanisms correspond to almost pure strike-slip faulting for both events. The events are located within the domain of the Austroalpine nappe system (Fig. 2b), in a seismically active region (Fig. 8). The observed strike-slip faulting is consistent with other mechanisms such as the  $M_L$  3.5 earthquake of January 2016, located about 9 km to the east of the 2018 events (Diehl et al. 2018).

### 3.3.3 *Herrischried (Germany) and Rhinegraben (France/Germany)*

On March 11, 2018, an  $M_L$  3.1 earthquake occurred close to the village of Herrischried in the Black Forest (HER, Fig. 2b). The focal depth of about 17 km is well constrained by stations in southern Germany. The focal mechanism is well constrained by polarities of P-wave first-motions (Fig. 7g) and corresponds to a strike-slip rupture with a normal-fault component. The mechanism is consistent with the “strike-slip to normal faulting” stress regime derived by Kastrup et al. (2004) for this part of the northern foreland.

Another strike-slip earthquake was located below the Rhinegraben in the border region between France and Germany on May 4, 2018 (RIG, Fig. 2b). With about 200

received felt reports, the  $M_L$  3.3 earthquake was felt by the population in northern Switzerland, especially in the region of Basel. The depth of 15 km and the strike-slip mechanism (Fig. 7i) are well constrained. This mechanism is similar to other solutions located in this depth level below the Rhinegraben (e.g., Kastrup et al. 2004).

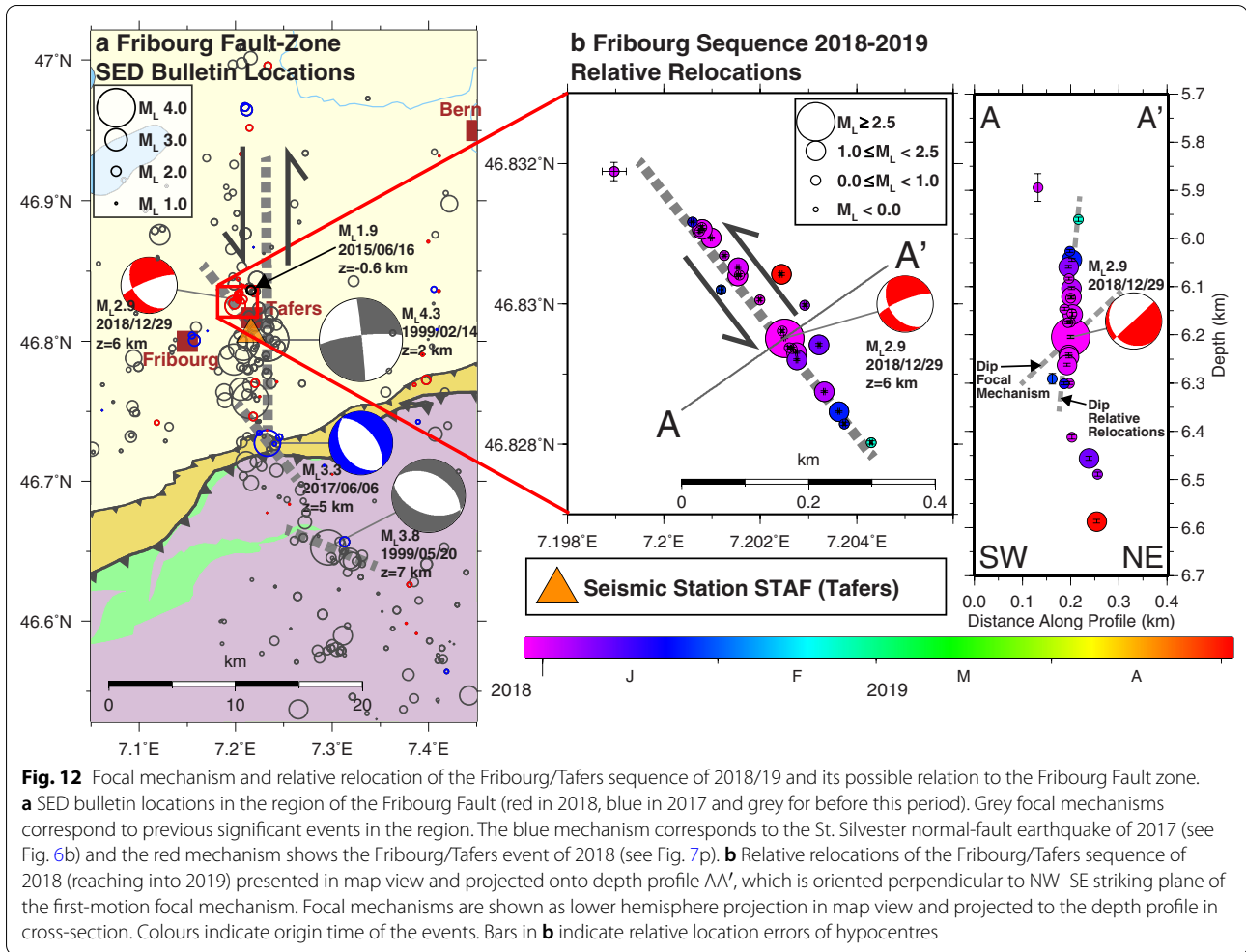
### 3.3.4 *Château-d’Oex (VD), 2018*

The focal mechanism of the  $M_L$  2.9 earthquake of April 8, 2018, located about 4.5 km SE of the Château d’Oex cluster active in 2017 and described above, is radically different from the extensional regime of this earlier cluster. In fact, the first-motion fault-plane solution of this event corresponds to an oblique reverse-faulting mechanism (Fig. 7h), with its P-axis oriented almost E–W. The derived depth of 5 km is only slightly higher by about 1 km than the bulk of the previous Château-d’Oex cluster.

The change from an extensional to a compressional focal mechanism within only a few kilometres implies either strong small-scale heterogeneities in the stress field or the activation of faults that are poorly oriented with respect to the far-field stress. In the first case, the differential stress available to activate a given fault is likely to be low. In either case, the occurrence of earthquakes with pronounced different focal mechanisms suggests that the faults are weak, a condition that is most easily met by the presence of fluids at near-lithostatic pressures (e.g. Sibson 1990, 2014).

### 3.3.5 *Châtel-St-Denis (FR)*

In addition to the St. Silvester and the two Château-d’Oex events of 2017 and 2018, the  $M_L$  3.1 Châtel-St-Denis earthquake of May 15, 2018 (CSD, Fig. 2a) represents the fourth significant earthquake that occurred in the Préalpes region during the reporting period. This  $M_L$  3.1 event is part of a small sequence of 6 additional earthquakes of  $M_L$  0.6–2.9, located about 3 km SW of Châtel-St-Denis between May and June 2018. For all these earthquakes the routinely determined source depth is 1–2 km. The closest observations of P- and S-phases are provided by the SSMNet station in Vevey (SVEJ), which is located at a distance of about 7 km from the epicentre. In case of the  $M_L$  3.1 event, we estimate the uncertainty of the 2 km focal depth to be on the order of  $\pm 2$ –3 km. We were able to compute a first-motion mechanism as well as a full moment tensor for the  $M_L$  3.1 event (Fig. 6f). The moment magnitude is  $M_W=3.1$  and the two focal mechanism agree remarkably well. The derived mechanism indicates predominantly normal faulting, which agrees to first order with the extensional mechanism of the St. Silvester and the 2017 Château-d’Oex event (Fig. 6) as well as with the Jaun event of 1999 (Fig. 12).



Similar to the St. Silvester earthquake of 2017 (Sect. 3.2.6), the Châtel-St-Denis epicentre locates at the boundary between subalpine Molasse and Préalpes nappes (Fig. 2b). According to the interpolated base-Mesozoic map of Sommaruga et al. (2012), the base of the Mesozoic cover lies at a depth of 3–3.5 km in the epicentral region. Assuming a vertical thickness of Mesozoic sediments of 2 km in this part of the Molasse basin (Sommaruga et al. 2012), Mesozoic sediments are expected between 1.0–1.5 and 3–3.5 km depth. A focal depth of 2 km therefore likely points to a source in the Mesozoic cover. However, with the current vertical uncertainty of  $\pm 2$ –3 km, a source in the subalpine Molasse or pre-Mesozoic basement, cannot be excluded.

### 3.3.6 Dent de Morcles (VS)

Two earthquakes of  $M_L$  2.6 (February 24) and  $M_L$  3.2 (August 23) happened close to the summit of the Dent de Morcles in 2018 (DDM, Fig. 2b). With about 400

received macroseismic felt reports, the  $M_L$  3.2 earthquake of August was widely felt by the population in the Rhone valley between Sion and Aigle. A few reports from the village of Collonges (epicentral distance 5 km) indicate a maximum intensity of degree V, likely related to amplification caused by the quaternary sediments of the Rhone valley. The focal depth of 6 km is well constrained by the dense network in this part of Switzerland and we estimate the uncertainty to be on the order of  $\pm 1$  km. The focal mechanisms of both events are relatively well constrained (Fig. 7e, f) and correspond to strike-slip faulting with a minor normal component. According to a profile of Pfiffner et al. (1997), which is located close to the epicentre region and based on the seismic reflection line W5 of the NRP-20 campaign, the depth of 6 km ( $\pm 1$  km) points to a source within the crystalline Aiguilles Rouge Massif west of the Rhone valley. An alternative interpretation of Steck et al. (1997) associates a band of SE dipping reflectors on the same W5 line with a sedimentary cover syncline separating

the Aiguilles-Rouge from the Infra-Rouge basement at depth. In their depth-migrated section, these reflectors locate between about 4 and 5.5–6.0 km depth in the hypocentral region of the Dent de Morcles earthquakes of 2018 (which projects near Collonges on the W5 profile). In this interpretation, the Dent de Morcles earthquakes would therefore locate near the top of the proposed Infra-Rouge basement and a source within the proposed Mesozoic cover syncline could not be entirely excluded. However, the interpretation of reflectors in the shallow part of the vibroseis and dynamite sections of line W5 is uncertain and debatable in the hypocentral region as described by Pfiffner et al. (1997).

The events locate about 13 km SSW of the 2004 earthquake sequence of Derborence, that marks the western end of the previously discussed earthquake lineament north of the Rhone valley (Anzère earthquakes, Sect. 3.3.1). The focal mechanisms of the Derborence and Dent de Morcles earthquakes are nearly identical (Baer et al. 2005). Moreover, the Dent de Morcles events are located about 8 km NE of the Martigny earthquake sequence of 2001 (Deichmann et al. 2002), which occurred on a NE–SW striking dextral strike-slip fault southeast of the Rhone valley. The Dent de Morcles earthquakes therefore indicate a possible link between the ENE–WSW striking lineament defined by epicentres located north of the Rhone valley and the NE–SW striking segment around Martigny (Fig. 8), which in turn might be linked to the Vallorcine segment located SW of Martigny. A kinematic connection in terms of a continuous dextral and slightly bent “Vallorcine-Valais shear zone” was proposed e.g. by Cara et al. (2017). Note, however, that the dextral planes in Fig. 7e, f strike WSW–ENE and therefore deviate from the general NE–SW trend in the alignment of the epicentres seen near Martigny. A possible explanation would again be the existence of en-echelon segments of strike-slip faults connecting the two larger fault systems to the NE and SW of the Martigny area. On the other hand, the along strike change of the alignment of epicentres in map view corresponds to the gentle bend of the Rhone-Simplon line possibly continuing into the “Chamonix/Mont Blanc shear zone” (CZ in Figs. 2 and 8) located between the Mont Blanc and Aiguille Rouge Massifs (e.g., Egli and Mancktelow 2013; Cara et al. 2017). Either way, the Dent de Morcles earthquakes of 2018 document ongoing strike-slip deformation likely located within the Aiguilles Rouge (or Infra-Rouge) Massif.

### 3.3.7 Martigny (VS)

The complexity in tectonic deformation within the bending zone between Central and Western Alps is

documented by the  $M_L$  2.9 earthquake that occurred on November 3, 2018, about 3 km SE of the town of Martigny (see MAR in Fig. 2b). Its epicentre locates about 12 km south from the Dent de Morcles events discussed in the previous section and about 3 km SE of Martigny. The depth of about 9 km is well constrained (uncertainty in the order of  $\pm 1$  km) and the event was widely felt along the Rhone valley, reaching an intensity of degree IV. The first-motion focal mechanism is very well constrained and corresponds to almost pure normal faulting. Its mechanism and the orientation of the T-axis is almost identical to the mechanism of the  $M_L$  3.3 earthquake that occurred in 1999, 15 km WNW, near Lac de Salanfe (Deichmann et al. 2000). The Martigny earthquake of 2018 very likely occurred within the crystalline basement of the Mont Blanc Massif, whereas the Lac de Salanfe earthquake was located at the northwestern rim of the Aiguille Rouges Massif neighbouring the base of the Morcles nappe. The T-axes are oriented NNE–SSW (Deichmann et al. 2000) and are consistent with the orientation of the T-axes of the strike-slip mechanisms of the Dent de Morcles and Vallorcine events discussed in the previous section, and differ only slightly from the N–S oriented T-axis of the strike-slip mechanism of the Martigny sequence of 2001. Given this relatively uniform orientation of the T-axes, the occurrence of both normal faulting and strike-slip earthquake mechanisms in close proximity to each other is not incompatible with a relatively uniform regional stress field indication a present-day transtensional regime within the bending zone between Central and Western Alps.

### 3.3.8 Fribourg/Tafers (FR)

On December 29, 2018, an  $M_L$  2.9 earthquake occurred northwest of Tafers, close to the city of Fribourg (FRI, Fig. 2b). Intensities of degree IV have been reported within a radius of about 7 km around the epicentre. The focal depth of 6 km is well constrained by P- and S-wave arrivals observed at stations at distances of 2.6 and 5 km in Tafers (STAF) and Fribourg (SFRU). We estimate the focal-depth uncertainty to be on the order of  $\pm 1$  km. The derived first-motion focal mechanism in Fig. 7p corresponds to strike-slip faulting with a substantial normal-fault component. The dip of plane 1, however, is not well resolved. The earthquake locates within the Fribourg seismicity cluster (Fig. 12a). The Fribourg Fault (FF in Fig. 2), associated with this cluster, was imaged as a N–S striking sinistral strike-slip fault zone within the sedimentary cover of the Molasse basin (e.g., Kastrup et al. 2007; Vouillamoz et al. 2017). The 2018 event differs in two aspects from other earthquakes along the Fribourg Fault, such as the  $M_L$  4.3 event of 1999 (Fig. 12a). First, the sinistral plane of the focal-plane solution strikes

NW–SE rather than N–S (Fig. 12a) and second, the depth of 6 km indicates a source in the pre-Mesozoic basement rather than in the sedimentary cover. To determine the active fault plane, we performed relative relocations for a subset of 23 events ( $M_L$  0.5–2.1) that followed the  $M_L$  2.9 earthquake between December 2018 and May 2019. The result of the relative relocation is shown in Fig. 12b in map view and along a vertical cross-section, oriented perpendicular to the sinistral plane of the focal mechanism. The NW–SE alignment of the relocated seismicity in Fig. 12b confirms the sinistral plane as the active plane. However, the dip imaged by the relative relocation in cross-section AA' indicates a sub-vertical fault plane (Fig. 12b), which deviates from the corresponding focal-plane solution of Fig. 7p. This discrepancy might be explained by the considerable uncertainty in dip of the corresponding focal plane and we therefore consider a sub-vertical sinistral fault as more likely.

In comparison with structural models of the uppermost crust in the region of the Fribourg Fault (e.g., Vouillamoz et al. 2017; Sommaruga et al. 2012), the depth of 6 km ( $\pm 1$  km) suggests a source in the crystalline basement. Additional evidence is provided by the seismogram recorded at station STAF at a distance of 2.6 km from the epicentre. The vertical component (HGZ) in Additional file 1: Figure S2 shows a prominent phase arriving between Pg and Sg onsets. We interpret this phase as an S-to-P (Sp) converted precursor phase, generated at the basement-sediment contrast by an Sg phase incident from below. We also compared the waveform of the 2018 event with waveforms of a shallow (depth – 0.6 km)  $M_L$  1.9 earthquake, which occurred in June 2015 in the same area likely within the sedimentary cover (Additional file 1: Figure S2). Although in a similar epicentral distance from station STAF, the shallow event indicates a 0.5 s shorter S-P time and the vertical component lacks the Sp phase, visible for the 2018 event (Additional file 1: Figure S2). The presence of the Sp phase in the 2018 event therefore suggests a NW–SE striking sinistral fault segment within the uppermost crystalline basement in the area of the Fribourg Fault. The NW–SE strike of the segment in the basement deviates from the general N–S trend previously proposed for the Fribourg Fault in the near-surface sedimentary cover. This deviation suggests that we are seeing two separate faults, activated by a common stress field with a maximum compressive stress oriented NNW–SSE. In addition, the observed difference in strike might indicate possible structural complexity of the strike-slip fault system, including the possibility of a soft-linkage between faults in the basement and faults in the overlaying sediments. The close proximity in space and time of the more recent events relative to the previous activity along the N–S trending Fribourg Fault Zone

could be due to stress transfer from the deformation of the near-surface lithology to the uppermost basement.

### 3.4 Seismicity associated with the former Deep Heat Mining project in Basel

In 2017, routine processing detected 12 earthquakes with magnitudes between  $M_L$  0.5 and  $M_L$  1.7. An additional 16 locatable earthquakes, with magnitudes between  $M_L$  0.0 and  $M_L$  0.6, were detected by template matching (Herrmann et al. 2019). The located events during this period occurred at the upper northern and upper southern periphery of the known seismic cloud (Additional file 1: Figure S3). The events occurred in or beyond regions of the seismic cloud that had last been active in December 2007. The seismic cloud was growing laterally and upward, away from the former injection point in 4.5 km depth. Specifically, the extension of the seismicity to the north had not been observed in the past years, when the seismicity occurred in other parts of the seismic cloud (Diehl et al. 2018).

In an analysis of the phenomenon, the SED concluded that the increasing overpressure, which started after the borehole's shut-in in April 2011, could be driving the seismicity in the geothermal reservoir (Wiemer et al. 2017). In Summer 2017, the well was bled off in a controlled, step-wise procedure: between July and October 2017. By the end of October 2017, the wellhead overpressure had been reduced completely, and the borehole has since remained open. Between May 2017 and the end of 2018, only one earthquake was strong enough to be reliably located ( $M_L$  0.7, in December 2017). It locates in the upper northern periphery of the seismic cloud and is the shallowest event of the events there (Additional file 1: Figure S3). All other events in this period, had magnitudes below  $M_L$  0.2.

### 3.5 Rockfalls and rock avalanches in 2017/18

On August 23 2017, at 7:30 UTC (9:30 a.m. local time), a large rock-slope failure occurred on the upper flanks of Pizzo Cengalo, at the head of the Bondasca Valley in Graubünden. This catastrophic event included the initial rock slope failure, a subsequent rock avalanche that travelled for 3.2 km, and generated a near-immediate debris flow. 8 hikers on a trail over run by the avalanche lost their lives. The debris flow caused significant damage in the village of Bondo, including damage to nearly 100 dwellings, 6 km down-valley of the slide area. The seismic waves generated by this sequence were observed as very broadband signals that exceeded periods of 100 s. Walter et al. (2020) detail the seismic waves generated by this event and estimate the failure to include  $3.0 \times 10^6$  m<sup>3</sup> of rock. The equivalent local magnitude related to the excited seismic waves of the rock fall and subsequent rock avalanche was  $M_L$  3.0.



The first seismic observation of rockslide activity on Pizzo Cengalo occurred on 27 December 2011, when a slide of  $1.5 \times 10^6 \text{ m}^3$  rock volume occurred, that had an equivalent local magnitude event of  $M_L$  2.8 (Deichmann et al. 2012) and also activated a similarly long runout rock avalanche. In 2016, this instability was activated again, with a rockslide event with equivalent magnitude of  $M_L$  2.1 (Diehl et al. 2018). Only 2 days before the largest event, at 9:31 UTC on 21 August 2017, a precursory rockslide was also observed by the network, with equivalent local magnitude event of  $M_L$  2.3. In the immediate aftermath of the  $M_L$  3.0 event, numerous slides were observed, and the seismic network could detect and locate 2 additional events at 9:04 and 9:36 UTC, with  $M_L$  1.3 and  $M_L$  2.1 respectively. On 15 September 2017, over 3 weeks later, an  $M_L$  2.8 rockslide on the mountain was again observed.

The seismic signals of the main event and these secondary slides are presented in Fig. 13, showing records from the 2 closest stations, VDL and TUE, located between 25 and 30 km distance from Pizzo Cengalo. The distinct signatures of the slide and subsequent mudslides—that continued to be re-activated independent of slide activity for days after then event—are seen in the seismic data. Walter et al. (2020) include waveform modelling of the main event as recorded at nearby stations. On 6 September 2017, a temporary seismic station with short period and accelerometer sensors (XP.PICE1) was placed within 2 km of the slide area at the Sciora Hut. This station operated beyond 2018.

#### 4 Discussion and conclusion

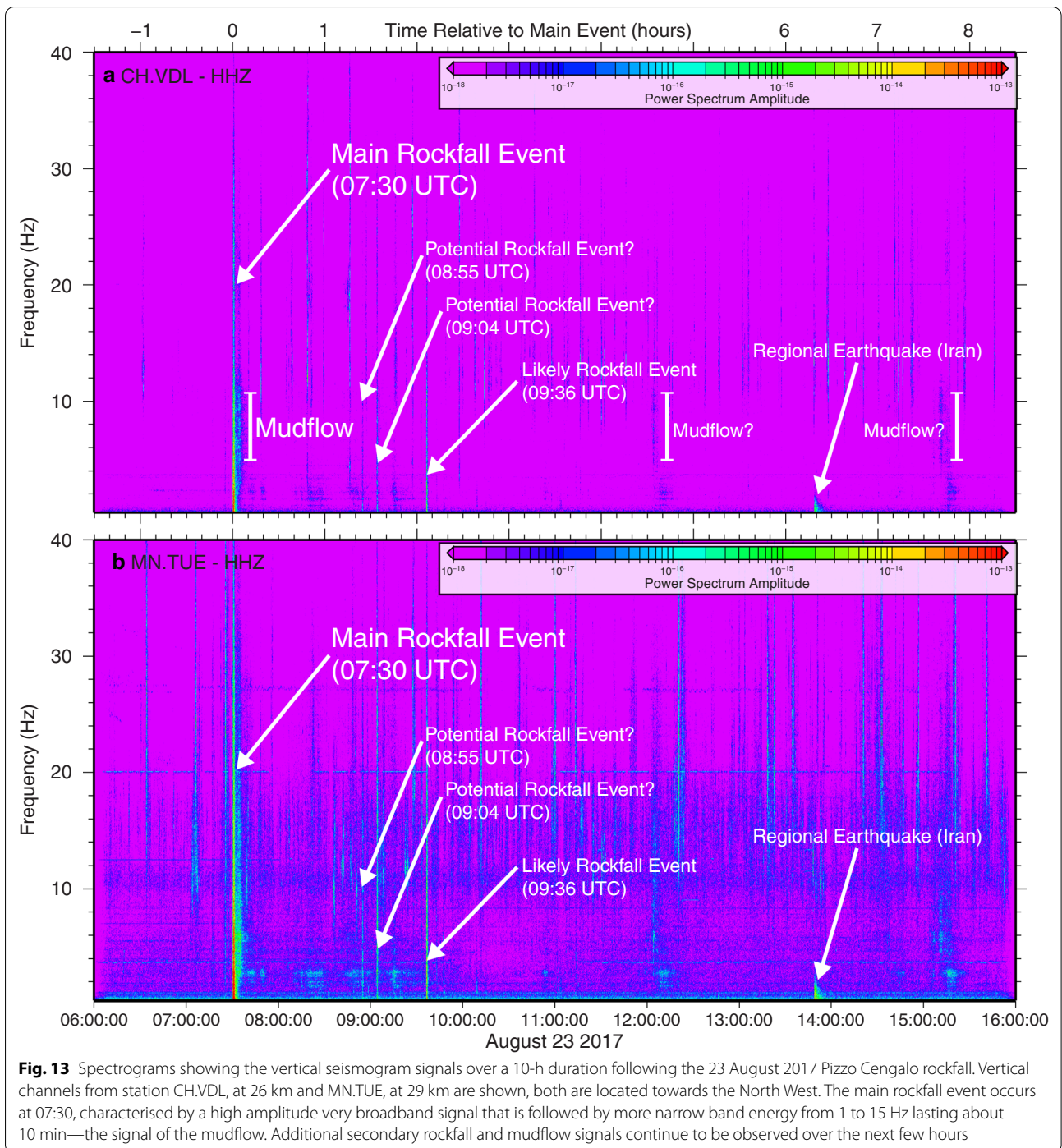
As discussed in Diehl et al. (2015, 2018), the total number of located earthquakes per year has increased since 2013 due to ongoing densification of the seismic network, improvements in detection methods, and the occurrence of vigorous earthquake sequences. The same trend is observed for the period 2017/18 (Fig. 3). With 1227 located events, the total annual number of earthquakes in 2017 was the highest so far recorded by the SED. On the other hand, with a total of 23 and 25 earthquakes of magnitude  $M_L \geq 2.5$ , the seismic activity of potentially felt events in either year was close to the yearly average of 23 earthquakes in the same magnitude range over the previous 42 years. The densification and improvement of the seismic network also results in an ever-increasing number of high-quality focal-plane solutions (42 in 2017/18), which allows more detailed and complete seismotectonic interpretations.

The strongest earthquake in the reporting period was the  $M_L$  4.6 Urnerboden earthquake of March 2017 (URB, Fig. 2a). Together with previous seismicity in this area, the earthquake images arrays of active, N–S to NNW–SSE oriented strike-slip faults, located within the

northern front of the uppermost Aar Massif. The strike-slip deformation in this part of the Aar Massif might be related to along-strike differences in the uplift history of the Aar Massif (e.g., Nibourel 2019).

Another remarkable earthquake sequence occurred in the Préalpes region close to Château-d'Oex (CDO, Fig. 2a), which culminated in an  $M_L$  4.3 earthquake in July 2017. Template-matching methods reveal several phases of increased activity since at least the year 2007. Similar complex, long-lasting sequences have been observed in Switzerland and surrounding regions before and are therefore not uncommon. Recent examples for similar sequences with bursts of activities over several years are the Diemtigen (Diehl et al. 2015) and the St. Léonard sequence (Diehl et al. 2018). The focal mechanism and relative relocations document NNE–SSW directed extension below the basal thrust of the Préalpes Médiannes. Most likely, the sequence is located near the top of the pre-Mesozoic basement. However, focal-depth uncertainties of  $\pm 1$ –2 km and uncertainties of geological models also allow a source within the autochthonous Mesozoic cover.

In 2017/18, two other events (St. Silvester, Châtel-St-Denis, Fig. 2) occurred along the northern boundary of the Préalpes nappes with predominantly normal-faulting mechanisms, indicating approximately NE–SW oriented extension similar to the Château-d'Oex sequence of 2017. All three extensional to transtensional events occurred near the top of the pre-Mesozoic basement, although, with the current uncertainties in focal depth and structural models, sources within the Mesozoic cover cannot be entirely ruled out. So far, information from focal mechanisms along the Alpine front in western Switzerland was sparse. For instance, the stress inversion of Kastrup et al. (2004) included not a single mechanism in this part of Switzerland. Delacou et al. (2004) included the normal-fault mechanism of the  $M_L$  3.8 Jaun earthquake of May 1999 (Fig. 12a) and a predominantly normal-fault mechanism in the Chablais region south of Lake Geneva ( $M_L$  4.8; 1968/08/19) in a stress analysis of the Central and Western Alps. Based on these two earthquakes, their resulting interpolated map of deformation shows a tendency for an extensional to transtensional regime in the Préalpes region in western Switzerland. Our three additional mechanisms therefore provide important new constraints and confirm the previous indications of Delacou et al. (2004) for a present-day extensional to transtensional deformation regime along the Alpine front in western Switzerland. This extension is approximately parallel to the strike of the Alpine front and consistent with orientations of minimum principal stresses reported by Kastrup et al. (2004) for western Switzerland. The extensional to transtensional regime along the Alpine front in western



Switzerland contrasts the strike-slip to thrust regime observed along the Alpine front in eastern Switzerland (Kastrup et al. 2004; Marschall et al. 2013) and might be related to uplift and extensional processes in the transition zone of Central and Western Alps. The thrust-fault event of 2018, located in close proximity to the Château d'Oex sequence of 2017, stands in contrast to the

observed regional extension regime, and as such could be symptomatic for the localized presence of fluids at near-lithostatic pressures.

As in previous years, a large portion of the seismic activity was concentrated in the Valais region in southwestern Switzerland (Fig. 2). Previous seismicity clusters like Vallorcine (VAL), as well as the St-Léonard (STL)

and Crans (CRA) sequences (Diehl et al. 2018), both located north of the Rhone valley, continued to be active also in 2017/18 (Fig. 2). The Dent de Morcles (DDM) earthquakes of 2018 (Fig. 2b) document strike-slip deformation within the Aiguilles Rouge Massif. The deformation locates north of the Rhone-Simplon Line (RSL) and the strike of the dextral plane is rotated clockwise with respect to the RSL, suggesting an en-echelon system of basement faults as proposed for segments farther to the east along the RSL (Diehl et al. 2018). Due to the dense station coverage in the Rhone valley, a focal mechanism for an  $M_L$  0.9 earthquake could be derived, which occurred right under the city of Sion in about 8 km depth in September 2018 (SIO, Fig. 2b, Additional file 1: Figure S1g). The predominantly strike-slip mechanism represents a rare example of strike-slip deformation in the centre of the Rhone valley and might be evidence for dextral strike-slip faulting along the RSL.

In the northern Alpine foreland, the Fribourg earthquake of December 2018 (FRI, Fig. 2b) reveals additional complexity along the Fribourg Fault Zone. The imaged fault segment likely locates in the basement and its strike deviates from the general N–S trend of the Fribourg Fault in the sedimentary cover. This segment might therefore indicate a possible soft-linkage between faults in the basement and faults in the overlying sediments. Finally, the Grenchen earthquake of 2017 (GRE, Fig. 2a) represents a rare example of ongoing shallow thrust faulting along the southern margin of the Jura fold-and-thrust belt, indicating seismically active contraction in the northwestern Alpine foreland of Switzerland.

## Supplementary Information

The online version contains supplementary material available at <https://doi.org/10.1186/s00015-020-00382-2>.

**Additional file 1.** Supporting information in form of additional four tables and three figures.

## Acknowledgements and Funding

Comments by Jon Mosar and Stefan Schmid helped to improve the manuscript and are thankfully acknowledged. We thank Herfried Madritsch for helpful discussions. We acknowledge international collaboration with our colleagues at the *Zentralanstalt für Meteorologie und Geodynamik* in Vienna (ZAMG, network code OE, <https://doi.org/10.7914/SN/OE>), the *Istituto Nazionale di Geofisica e Vulcanologia* in Rome (INGV, network code IV, <https://doi.org/10.13127/SD/X0FXNH7QFY>), the *Istituto di Geofisica, Università di Genova* (network code GU, <https://doi.org/10.7914/SN/GU>), the *Zivilschutz der Autonomen Provinz Bozen-Südtirol* (network code SI), the *Istituto Nazionale di Oceanografia e di Geofisica Sperimentale* (OGS, network code OX, <https://doi.org/10.7914/SN/OX>) in Trieste, the *Landeserdbebendienst Baden-Württemberg* in Freiburg (LED, network code LE), the *Bundesanstalt für Geowissenschaften und Rohstoffe* in Hannover (BGR, network code GR, <https://doi.org/10.25928/mbx6-hr74>), and the *Réseau Sismologique et Géodésique Français* (RESIF, network code FR, <http://dx.doi.org/10.15778/RESIF.FR> and RA, <https://doi.org/10.15778/RESIF.RA>).

The authors especially thank the SED Electronic Laboratory team, who build and maintain the seismic network, and Stefan Heimers, Roman Racine

and Luca Scarabello who maintain and develop the hardware and software infrastructure of the seismic network.

Financial support from the Nationale Genossenschaft für die Lagerung radioaktiver Abfälle (Nagra) for the operation of several stations in northern Switzerland and the research presented in this study is gratefully acknowledged. We thank SwissEnergy ([www.energieschweiz.ch](http://www.energieschweiz.ch)) and the Swiss Federal Office of Energy ([www.bfe.admin.ch](http://www.bfe.admin.ch)) for the financial support of projects GEOBEST-CH/2 and SIAMIS-GT. We acknowledge additional funding and support for instrumentation by the Swiss Competence Center for Energy Research—Supply of Electricity ([www.sccer-soe.ch](http://www.sccer-soe.ch)), St. Galler Stadtwerke (sgsw), Services Industriels de Genève (SIG), Alpine Geothermal Power Production SA (AGEPP), Kanton Basel Stadt and Industrielle Werke Basel (IWB).

We acknowledge the AlpArray Seismic Network Team ([http://www.alparay.ethz.ch/seismic\\_network/backbone/management/](http://www.alparay.ethz.ch/seismic_network/backbone/management/)) who maintain the AlpArray Seismic Network (network code Z3, [https://doi.org/10.12686/alparay/z3\\_2015](https://doi.org/10.12686/alparay/z3_2015)). AlpArray Switzerland is funded by the Swiss-AlpArray SINERGIA project CRSII2\_154434/1 by Swiss National Science Foundation (SNSF).

## Authors' contributions

TD computed magnitude of completeness maps, focal mechanisms, moment tensors, relative relocations, prepared figures and crafted and wrote the main manuscript. JC manages the seismic network and supervises the renewal of the SDSNet, contributed to the analysis of seismicity, contributed text to the main manuscript. CC computed ShakeMaps and contributed figures on ground-motion and text to main manuscript. TK contributed to analysis of seismicity, prepared figures and text for main manuscript and Additional file. PK analysed the macroseismic data presented in this study. ND contributed to the seismotectonic interpretation. FM contributed to the analysis of seismicity and translations. FG, IM, MB contributed to the analysis of seismicity. MH is responsible for the renewal of the strong-motion network and contributed with fieldwork. FH contributed with text and proofreading. As head of SED's Risk & Hazard group, DF supervises the renewal of the strong-motion network and other products presented in this study. As the director of the SED, SW provided supervision of the research, and contributed with text and proofreading. All authors reviewed the manuscript. All authors read and approved the final manuscript.

## Availability of data and materials

SED seismic network data used in this report is collected under permanent network code CH (<https://doi.org/10.12686/sed/networks/ch>) and temporary network codes 8D (<https://doi.org/10.12686/sed/networks/8d>), 4D (<https://doi.org/10.12686/sed/networks/4d>), XP (<https://doi.org/10.12686/sed/networks/xp>) and XY (<https://doi.org/10.12686/sed/networks/xy>). The CERN seismic network consists of 3 stations under network code C4 (<https://doi.org/10.12686/sed/networks/c4>). Waveform data from the SED permanent seismic network (network codes CH) as well as the majority of data collected by collaborating networks (network codes as in Acknowledgements) in the greater Alpine region are openly available through the European Integrated Data Archive (EIDA): <http://www.orfeus-eu.org/data/eida/>. The majority of data collected by temporary networks in the framework of Ph.D. studies or in collaboration with industry is restricted or embargoed.

## Ethics approval and consent to participate

Not applicable.

## Consent for publication

Not applicable.

## Competing interests

The authors declare that they have no competing interests.

## Author details

<sup>1</sup> Swiss Seismological Service, ETH Zürich, Sonneggstrasse 5, 8092 Zürich, Switzerland. <sup>2</sup> Department of Earth Sciences, Institute of Geophysics, ETH Zürich, Zürich, Switzerland. <sup>3</sup> Present Address: Istituto Nazionale di Geofisica e Vulcanologia, Sezione di Bologna, Bologna, Italy.

Received: 13 September 2020 Accepted: 25 November 2020  
Published online: 11 February 2021



## References

- Aki, K., & Richards, P. G. (2002). *Quantitative seismology* (2nd ed., p. 704). Mill Valley: University Science Books.
- AlpArray Seismic Network. (2015). *AlpArray Seismic Network (AASN) temporary component*. AlpArray Working Group. Other/Seismic Network. [https://doi.org/10.12686/alparray/z3\\_2015](https://doi.org/10.12686/alparray/z3_2015).
- Bachura, M., & Fischer, T. (2019). Waveform cross-correlation for differential time measurement: Bias and limitations. *Seismological Research Letters*, 90(5), 2005–2014. <https://doi.org/10.1785/0220190096>.
- Baer, M., Deichmann, N., Braunmiller, J., Husen, S., Fäh, D., Giardini, D., et al. (2005). Earthquakes in Switzerland and surrounding regions during 2004. *Ecolgae Geologicae Helvetiae*, 98(3), 407–418.
- Cara, M., Van der Woerd, J., Alasset, P.-J., Benjumea, J., & Mériaux, A.-S. (2017). The 1905 Chamonix earthquakes: Active tectonics in the Mont Blanc and Aiguilles Rouges massifs. *Swiss Journal of Geosciences*, 110, 631–651. <https://doi.org/10.1007/s00015-017-0262-7>.
- Cauzzi, C., Edwards, B., Fäh, D., Clinton, J., Wiemer, S., Kästli, P., et al. (2015). New predictive equations and site amplification estimates for the next-generation Swiss ShakeMaps. *Geophysical Journal International*, 200, 421–438. <https://doi.org/10.1093/gji/ggu404>.
- Cauzzi, C., Sleeman, R., Clinton, J., et al. (2016). Introducing the European rapid raw strong-motion database. *Seismological Research Letters*, 35, 1671–1690. <https://doi.org/10.1785/0220150271>.
- Clinton, J., Cauzzi, C., Fäh, D., Michel, C., Zweifel, P., Olivieri, M., et al. (2011). The current state of strong motion monitoring in Switzerland. In S. Akkar, P. Gülkan, & T. van Eck (Eds.), *Earthquake data in engineering seismology: Predictive models, data management and networks (geotechnical, geological and earthquake engineering)*. New York: Springer.
- Deichmann, N., Baer, M., Braunmiller, J., Ballarin Dolfin, D., Bay, F., Bernardi, F., et al. (2002). Earthquakes in Switzerland and surrounding regions during 2001. *Ecolgae Geologicae Helvetiae—Swiss Journal of Geosciences*, 95(2), 249–261.
- Deichmann, N., Baer, M., Braunmiller, J., Ballarin Dolfin, D., Bay, F., Delouis, B., et al. (2000). Earthquakes in Switzerland and surrounding regions during 1999. *Ecolgae Geologicae Helvetiae*, 93(3), 395–406.
- Deichmann, N., Baer, M., Braunmiller, J., Cornou, C., Fäh, D., Giardini, D., et al. (2004). Earthquakes in Switzerland and surrounding regions during 2003. *Ecolgae Geologicae Helvetiae—Swiss Journal of Geosciences*, 97(3), 447–458.
- Deichmann, N., Baer, M., Braunmiller, J., Husen, S., Fäh, D., Giardini, D., et al. (2006). Earthquakes in Switzerland and surrounding regions during 2005. *Ecolgae Geologicae Helvetiae—Swiss Journal of Geosciences*, 99(3), 443–452. <https://doi.org/10.1007/s00015-006-1201-1>.
- Deichmann, N., Baer, M., Clinton, J., Husen, S., Fäh, D., Giardini, D., et al. (2008). Earthquakes in Switzerland and surrounding regions during 2007. *Swiss Journal of Geosciences*, 101(3), 659–667. <https://doi.org/10.1007/s00015-008-1304-y>.
- Deichmann, N., Clinton, J., Husen, S., Edwards, B., Haslinger, F., Fäh, D., et al. (2012). Earthquakes in Switzerland and surrounding regions during 2011. *Swiss Journal of Geosciences*, 105, 463–476. <https://doi.org/10.1007/s00015-012-0116-2>.
- Delacou, B., Sue, C., Champagnac, J.-D., & Burkhard, M. (2004). Present-day geodynamics in the bend of the western and central Alps as constrained by earthquake analysis. *Geophysical Journal International*, 158(2), 753–774. <https://doi.org/10.1111/j.1365-246X.2004.02320.x>.
- Diehl, T., Clinton, J., Deichmann, N., Cauzzi, C., Kästli, P., Kraft, T., et al. (2018). Earthquakes in Switzerland and surrounding regions during 2015 and 2016. *Swiss Journal of Geosciences*. <https://doi.org/10.1007/s00015-017-0295-y>.
- Diehl, T., Clinton, J., Kraft, T., Husen, S., Plenkers, K., Guilhelm, A., et al. (2014). Earthquakes in Switzerland and surrounding regions during 2013. *Swiss Journal of Geosciences*, 107, 359–375. <https://doi.org/10.1007/s00015-014-0171-y>.
- Diehl, T., Deichmann, N., Clinton, J., Husen, S., Kraft, T., Plenkers, K., et al. (2013). Earthquakes in Switzerland and surrounding regions during 2012. *Swiss Journal of Geosciences*, 106, 543–558. <https://doi.org/10.1007/s00015-013-0154-4>.
- Diehl, T., Deichmann, N., Clinton, J., Kästli, P., Cauzzi, C., Kraft, T., et al. (2015). Earthquakes in Switzerland and surrounding regions during 2014. *Swiss Journal of Geosciences*, 108, 425–443. <https://doi.org/10.1007/s00015-015-0204-1>.
- Diehl, T., Kraft, T., Kissling, E., & Wiemer, S. (2017). The induced earthquake sequence related to the St. Gallen deep geothermal project (Switzerland): Fault reactivation and fluid interactions imaged by microseismicity. *Journal of Geophysical Research: Solid Earth*, 122, 7272–7290. <https://doi.org/10.1002/2017JB014473>.
- Edwards, B., Allmann, B., Fäh, D., & Clinton, J. (2010). Automatic computation of moment magnitudes for small earthquakes and the scaling of local to moment magnitude. *Geophysical Journal International*, 183(1), 407–420. <https://doi.org/10.1111/j.1365-246X.2010.04743.x>.
- Edwards, B., & Fäh, D. (2013). A stochastic ground-motion model for Switzerland. *Bulletin of the Seismological Society of America*, 103, 78–98. <https://doi.org/10.1785/0120110331>.
- Egli, D., & Mancktelow, N. (2013). The structural history of the Mont Blanc massif with regard to models for its recent exhumation. *Swiss Journal of Geosciences*, 106(3), 469–489. <https://doi.org/10.1007/s00015-013-0153-5>.
- Faenza, L., & Michelini, A. (2010). Regression analysis of MCS intensity and ground motion parameters in Italy and its application in ShakeMap. *Geophysical Journal International*, 180, 1138–1152. <https://doi.org/10.1111/j.1365-246X.2009.04467.x>.
- Fäh, D., Giardini, D., Kästli, P., Deichmann, N., Gisler, M., Schwarz-Zanetti, G., Alvarez-Rubio, S., Sellami, S., Edwards, B., Allmann, B., Bethmann, F., Woessner, J., Gassner-Stamm, G., Fritsche, S., & Eberhard, D. (2011). *ECOS-09 earthquake catalogue of Switzerland release 2011 report and database, Public catalogue*, 17. 4. 2011. Swiss Seismological Service ETH Zurich, Report SED/RISK/R/001/20110417.
- Fréchet, J., Thouvenot, F., Frogneux, M., Deichmann, N., & Cara, M. (2010). The  $M_w$  4.5 Vallorcine (French Alps) earthquake of 8 September 2005 and its complex aftershock sequence. *Journal of Seismology*, 15, 43–58. <https://doi.org/10.1007/s10950-010-9205-8>.
- Goertz-Allmann, B. P., Edwards, B., Bethmann, F., Deichmann, N., Clinton, J., Fäh, D., & Giardini, D. (2011). A new empirical magnitude scaling relation for Switzerland. *Bulletin of the Seismological Society of America*, 101(6), 3088–3095. <https://doi.org/10.1785/0120100291>.
- Gruber, M. (2017). Structural investigations of the Western Swiss molasse basin: from 2D seismic interpretation to a 3D geological model. *Ph.D. Thesis*, No. 2029, University of Fribourg, Switzerland.
- Grünthal, G. (1998). European Macroseismic Scale 1998 (EMS-98). Cahiers du Centre Européen de Géodynamique et de Séismologie 15, Centre Européen de Géodynamique et de Séismologie, Luxembourg, pp. 99.
- Hardebeck, J. L., & Shearer, P. M. (2002). A new method for determining first-motion focal mechanisms. *Bulletin of the Seismological Society of America*, 92, 2264–2276.
- Herrmann, M., Kraft, T., Tormann, T., Scarabello, L., & Wiemer, S. (2019). A consistent high-resolution catalog of induced seismicity in Basel based on matched filter detection and tailored post-processing. *Journal of Geophysical Research: Solid Earth*. <https://doi.org/10.1029/2019JB017468>.
- Heuberger, S., Roth, P., Zingg, O., Naef, H., & Meier, B. P. (2016). The St. Gallen Fault Zone: A long-lived, multiphase structure in the North Alpine Foreland Basin revealed by 3D seismic data. *Swiss Journal of Geosciences*, 109(1), 83–102. <https://doi.org/10.1007/s00015-016-0208-5>.
- Husen, S., & Hardebeck, J. L. (2010). Earthquake location accuracy. *Community Online Resource for Statistical Seismicity Analysis*. <https://doi.org/10.5078/corssa-55815573>.
- Husen, S., Kissling, E., Deichmann, N., Wiemer, S., Giardini, D., & Baer, M. (2003). Probabilistic earthquake location in complex three-dimensional velocity models: Application to Switzerland. *Journal of Geophysical Research*, 108(B2), 2077–2096.
- Kastrup, U., Deichmann, N., Fröhlich, A., & Giardini, D. (2007). Evidence for an active fault below the northwestern Alpine foreland of Switzerland. *Geophysical Journal International*, 169(3), 1273–1288. <https://doi.org/10.1111/j.1365-246X.2007.03413.x>.
- Kastrup, U., Zoback, M.-L., Deichmann, N., Evans, K., Giardini, D., & Michael, A. J. (2004). Stress field variations in the Swiss Alps and the northern Alpine foreland derived from inversion of fault plane solutions. *Journal of Geophysical Research*. <https://doi.org/10.1029/2003JB002550B01402>.
- Lanza, F., Diehl, T., Deichmann, N., Kraft, T., & Wiemer, S. (2020). *Seismological analysis of the last 20 years of natural seismicity in the vicinity of the Mont Terri Rock Lab*. Technical Report, Swiss Seismological Service.
- Lanza, F., Diehl, T., Kraft, T., Deichmann, N., Wiemer, S., Nussbaum, C., & Schefer, S. (2019). *Seismotectonic analysis of seismicity in the vicinity of the Mont Terri rock lab*. 17th Swiss Geoscience Meeting, Fribourg, 2019.



- Lomax, A., Virieux, J., Volant, P., & Thierry-Berge, C. (2000). Probabilistic earthquake location in 3D and layered models. In C. H. Thurber & N. Rabinowitz (Eds.), *Advances in seismic event location* (pp. 101–134). London: Kluwer Academic Publishers.
- Marschall, I., Deichmann, N., & Marone, F. (2013). Earthquake focal mechanisms and stress orientations in the eastern Swiss Alps. *Swiss Journal of Geosciences*, 106, 79–90. <https://doi.org/10.1007/s00015-013-0129-5>.
- Matzenauer, E. (2012). Tectonics of the Préalpes Klippen and the subalpine molasse (canton Fribourg, Switzerland). *Ph.D. Thesis*, No. 1737, University of Fribourg, Switzerland.
- Maurer, H. R., Burkhard, M., Deichmann, N., & Green, A. G. (1997). Active tectonism in the central Alps: Contrasting stress regimes north and south of the Rhone Valley. *Terra Nova*, 9(2), 91–94.
- Meier, B. P. (2010). Ergänzende interpretation reflexionsseismischer Linien zwischen dem östlichen und westlichen Molassebecken. *Nagra Arbeitsbericht* (vol. NAB 10–40, pp. 48) Nagra, Wettingen, Switzerland.
- Michel, C., Edwards, B., Poggi, V., Burjanek, J., Roten, D., Cauzzi, C., & Fäh, D. (2014). Assessment of site effects in Alpine regions through systematic site characterization of seismic stations. *Bulletin of the Seismological Society of America*, 104, 2809–2826. <https://doi.org/10.1785/0120140097>.
- Mock, S., & Herwegh, M. (2017). Tectonics of the central Swiss Molasse Basin: Post-Miocene transition to incipient thick-skinned tectonics? *Tectonics*. <https://doi.org/10.1002/2017TC004584>.
- Molinari, I., Clinton, J., Kissling, E., Hetényi, G., Giardini, D., Stipčević, J., et al. (2016). Swiss-AlpArray temporary broadband seismic stations deployment and noise characterization. *Advances in Geosciences*, 43, 15–29. <https://doi.org/10.5194/adgeo-43-15-2016>.
- Mosar, J., Stampfli, G. M., & Girod, F. (1996). Western Préalpes Médiannes Romanides: Timing and structure. A review. *Eclogae Geologicae Helveticae*, 89, 389–425. <https://doi.org/10.5169/seals-167907>.
- Nanjo, K. Z., Schorlemmer, D., Woessner, J., Wiemer, S., & Giardini, D. (2010). Earthquake detection capability of the Swiss Seismic Network. *Geophysical Journal International*, 181, 1713–1724. <https://doi.org/10.1111/j.1365-246X.2010.04593.x>.
- Nibourel, L. (2019). The structural and thermo-kinetic evolution of the eastern Aar Massif, Switzerland. *Ph.D. Thesis*, University of Bern, Switzerland.
- Pagani, M., Monelli, D., Weatherill, G., et al. (2014). OpenQuake engine: An open hazard (and risk) software for the global earthquake model. *Seismological Research Letters*, 85, 692–702. <https://doi.org/10.1785/0220130087>.
- Pfiffner, O. A. (2014). *Geology of the Alps* (2nd ed.). New York: Wiley.
- Pfiffner, O. A., Sahli, S., et al. (1997). Structure and evolution of the external basement massifs (Aar, Aiguilles-Rouges/Mt. Blanc). In O. A. Pfiffner, et al. (Eds.), *Deep structure of the Alps, results of NRP20* (pp. 139–153). Basel: Birkhäuser.
- Schorlemmer, D., & Woessner, J. (2008). Probability of detecting an earthquake. *Bulletin of the Seismological Society of America*, 98(5), 2103–2217. <https://doi.org/10.1785/0120070105>.
- Sibson, R. (1990). Rupture nucleation on unfavorably oriented faults. *Bulletin of the Seismological Society of America*, 80(6), 1580–1604.
- Sibson, R. (2014). Earthquake rupturing in fluid-overpressured crust: How common. *Pure and Applied Geophysics*. <https://doi.org/10.1007/s00024-014-0838-3>.
- Singer, J., Diehl, T., Husen, S., Kissling, E., & Duretz, T. (2014). Alpine lithosphere slab rollback causing lower crustal seismicity in northern foreland. *Earth and Planetary Science Letters*, 397, 42–56. <https://doi.org/10.1016/j.epsl.2014.04.002>.
- Sommaruga, A., Eichenberger, U., & Marillier, F. (2012). *Seismic atlas of the swiss molasse basin*. Zurich: Swiss Geophysical Commission.
- Steck, A., Epard, J.-L., et al. (1997). Geological interpretation of the seismic profiles through Western Switzerland: Rawil (W1), Val d'Anniviers (W2), Mattertal (W3), Zmutt-Zermatt-Findelen (W4) and Val de Bagnes (W5). In O. A. Pfiffner, et al. (Eds.), *Deep structure of the Alps, results of NRP20* (pp. 123–137). Basel: Birkhäuser.
- Swiss Seismological Service (SED) at ETH Zurich. (1983). National Seismic Networks of Switzerland; *ETH Zürich*. Other/Seismic Network. <https://doi.org/10.12686/sed/networks/ch>.
- Swisstopo. (2005). *Tektonische Karte der Schweiz 1:500,000*. Wabern: Federal Office of Topography Swisstopo.
- Vouillamoz, N., Mosar, J., & Deichmann, N. (2017). Multi-scale imaging of a slow active fault zone: Contribution for improved seismic hazard assessment in the Swiss Alpine foreland. *Swiss Journal of Geoscience*, 110, 547. <https://doi.org/10.1007/s00015-017-0269-0>.
- Waldhauser, F., & Ellsworth, W. L. (2000). A double-difference earthquake location algorithm: Method and application to the northern Hayward fault, California. *Bulletin of the Seismological Society of America*, 90(6), 1353–1368. <https://doi.org/10.1785/0120000006>.
- Walter, F., Amann, F., Kos, A., Kenner, R., Phillips, M., de Preux, A., et al. (2020). Direct observations of a three million cubic meter rock-slope collapse with almost immediate initiation of ensuing debris flows. *Geomorphology*, 351, 106933. <https://doi.org/10.1016/j.geomorph.2019.106933>.
- Wells, D. L., & Coppersmith, K. J. (1994). New empirical relationships among magnitude, rupture length, rupture width, rupture area, and surface displacement. *Bulletin of the Seismological Society of America*, 84(4), 974–1002.
- Wiemer, S., Tormann, T., Herrmann, M., Karvounis, D., Kraft, T., & Marti, M. (2017). *Induzierte Erdbeben im Nachgang des eingestellten Geothermieprojekts in Basel*. Report of the Swiss Seismological Service, pp. 12. <https://doi.org/10.3929/ethz-b-000254199>.
- Worden, C. B., Thompson, E. M., Baker, J. W., et al. (2018). Spatial and spectral interpolation of ground-motion intensity measure observations. *Bulletin of the Seismological Society of America*, 108, 866–875. <https://doi.org/10.1785/0120170201>.
- Worden, C. B., Thompson, E. M., Hearne, M., & Wald, D. J. (2020). ShakeMap Manual Online: Technical manual, user's guide, and software guide, U. S. Geological Survey. <http://usgs.github.io/shakemap/>. <https://doi.org/10.5066/F7D21VPQ>.
- Worden, C. B., Wald, D. J., Allen, T. I., Lin, K., Garcia, D., & Cua, G. (2010). A revised ground-motion and intensity interpolation scheme for ShakeMap. *Bulletin of the Seismological Society of America*, 100, 3083–3096. <https://doi.org/10.1785/0120100101>.

## Publisher's Note

Springer Nature remains neutral with regard to jurisdictional claims in published maps and institutional affiliations.

**Submit your manuscript to a SpringerOpen® journal and benefit from:**

- Convenient online submission
- Rigorous peer review
- Open access: articles freely available online
- High visibility within the field
- Retaining the copyright to your article

Submit your next manuscript at ► [springeropen.com](https://www.springeropen.com)